Chemical Geology 639 (2023) 121724

Contents lists available at ScienceDirect

Chemical Geology

journal homepage: www.elsevier.com/locate/chemgeo

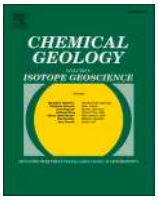

Decarbonation and clast dissolution timescales for short-term magma-carbonate interactions in the volcanic feeding system and their influence on eruptive dynamics: Insights from experiments at atmospheric pressure

M. Knuever [a,*], R. Sulpizio [a], D. Mele [a], A. Pisello [b], A. Costa [c], D. Perugini [b], F. Vetere [b,d]

[a] Università di Bari Aldo Moro, Dipartimento di Scienza della Terra e Geoambientali, Italy
[b] Università di Perugia, Dipartimento di Fisica e Geologia, Italy
[c] Istituto Nazionale di Geofisica e Vulcanologia (INGV) – Sezione di Bologna, Italy
[d] Università di Siena, Dipartimento di Scienze Fisiche, della Terra e dell'Ambiente, Italy

ARTICLE INFO

Editor: Dr Claudia Romano

Keywords:
Carbonate assimilation
Magma ascent
Explosive volcanism
Eruptive behaviour
Lithic erosion
Feeding dyke

ABSTRACT

While long-term interactions of magma with carbonate wall-rock (a.k.a. carbonate assimilation) are well-studied, only recently some experimental studies focused on short-term interactions (seconds to minutes) at magma chamber conditions (0.5 GPa and 1200 °C). They have shown that carbonate assimilation can effectively release CO_2 and dissolve the ingested clast in *syn*-eruptive timescales. Carbonate wall-rock xenoliths in eruptive products can hence be seen as proof of even shallower ingestion (i.e., within the feeding dyke). To study these shallower interactions, we performed 66 experiments at atmospheric pressure (i.e., at the second endmember of the volcanic feeding system) and at 950–1230 °C with varying melt compositions and limestone compositions. Decarbonation was found to be mainly dependent on temperature and limestone composition while clast dissolution is largely dependent on magma composition, temperature, pressure and interaction time. In natural systems during magma ascent and with increasing quantities of assimilated wall-rock, the magma temperature would steadily decrease, limiting its own decarbonation and assimilation ability. But even in the 950 °C-experiments decarbonation (i.e., CO_2 release) remained a *syn*-eruptive process. We subsequently discussed the limits of carbonate assimilation as well as the potential effect of *syn*-eruptive addition of CO_2 to the magmatic mixture on magma ascent and eruption dynamics.

1. Introduction

The interaction of magma with wall-rock is an unavoidable process during its ascent from the magma chamber to Earth's surface. The interaction with wall-rocks that can release volatile phases (i.e., mainly H_2O from sedimentary rocks or CO_2 from limestones) is of particular interest, since they might significantly alter eruption dynamics (Dallai et al., 2011; Freda et al., 2011; Pappalardo et al., 2018). The release of additional volatiles might even be the cause for the transition of effusive to explosive eruptive behaviour (Freda et al., 2011). Examples of geological settings where volcanoes sit on limestone or sedimentary basements include volcanoes like Colli Albani (di Rocco et al., 2012; Cross et al., 2014), El Hierro (Troll et al., 2012b), Merapi (Deegan et al., 2010; Troll et al., 2012a; Blythe et al., 2015), Pacaya (Janik et al., 1992), Popocatepetl (Goff et al., 2001), and Somma-Vesuvius (del Moro et al., 2001; Dallai et al., 2011; Jolis et al., 2013).

In general, the interaction between magma and wall-rocks may happen on two distinctive timescales: i) long-term interactions (lasting hours or more), which mostly occur in the deeper magmatic storage zone (i.e., sills or magma chambers with $P > 0.2$ GPa) as contact metamorphism, and ii) short-term interactions (lasting seconds to tens of minutes), correlating to magma ascent times (e.g., Costa et al., 2009b), which might occur in deeper storage zone settings as well as in shallower settings (i.e., within the feeding dyke or conduit with $P < 0.2$ GPa). Long-term magma-carbonate interaction (or carbonate assimilation) at the magma chamber level (i.e., $P > 0.2$ GPa) is already well-studied from many different angles, including experimentally, through rock and mineral geochemistry and through gas geochemistry (e.g.,

* Corresponding author at: Università degli Studi di Bari Aldo Moro, Dipartimento di Scienze della Terra e Geoambientali, Via E. Orabona 4, 70125 Bari (BA), Italy.
E-mail address: marco.knuever@uniba.it (M. Knuever).

https://doi.org/10.1016/j.chemgeo.2023.121724
Received 16 January 2023; Received in revised form 23 June 2023; Accepted 15 August 2023
Available online 14 September 2023

Chadwick et al., 2007; Iacono-Marziano et al., 2007, 2008, 2009; Freda et al., 2008; Mollo et al., 2010; Dallai et al., 2011; Troll et al., 2012a; Gozzi et al., 2014; Carter and Dasgupta, 2015, 2016; Whitley et al., 2019; Buono et al., 2020; Morris and Canil, 2022). Inversely, experimental studies on short-term carbonate assimilation are very limited but confirm how carbonate assimilation can be a *syn*-eruptive process at experimental p-T-conditions that are reflecting magma chamber conditions (1200 °C, 0.5–1 GPa; Deegan et al., 2010; Jolis et al., 2013; Blythe et al., 2015). Besides one study of Deegan et al. (2022) on magma-shale interactions (which included a large carbonate component) at 0.15 GPa no experimental data is available for shallower conditions ($P < 0.5$ GPa). While Deegan et al. (2010) and Jolis et al. (2013) were focussing on understanding the processes of magma-carbonate interactions at a distinct volcanic setting (Merapi and Somma-Vesuvius, respectively), Blythe et al. (2015) found, by comparing the results of the previous two, that melt viscosity might be the main controlling factor on carbonate assimilation rate. Deegan et al. (2022) found in the magma-shale experiments evidence for CO_2 release and fast chemical dissolution of the carbonate component of the shale into the magma. Carter and Dasgupta (2016) came to a similar conclusion from their longer duration experiments (24–96 h) with andesitic, dacitic, and rhyolitic starting materials. Iacono-Marziano et al. (2008) have shown that up to 20 wt% of limestones are dissolvable in hydrous basaltic melts (at 1050–1150 °C). Hence, from a geochemical standpoint, carbonate assimilation can serve as source for massive CO_2 production, which affects magma ascent and eruption dynamics.

To describe magma-carbonate interactions more precisely, we will follow the nomenclature introduced in Knuever et al. (2022), where the carbonate assimilation process is subdivided into three observable processes: i) the ingestion, which describes only the physico-mechanical process of entrainment of the clast into a magmatic body (by abrasion or erosion), ii) the decarbonation, which describes only the thermal decomposition due to heating above the crystallographic stability and the subsequent release of CO_2, and iii) the digestion or dissolution, which should refer to the chemical dissolution of the ingested clast via diffusive transport of Ca (± Mg) into the melt. Finally, assimilation will be used to describe the complete mechanical and chemical destruction of the carbonate xenoliths (i.e., when all the before mentioned processes are involved or concluded).

Very short decarbonation timescales have been inferred in several studies from thermal re-equilibration experiments or modelling (Sottili et al., 2010; Freda et al., 2011; Buono et al., 2020; Carr et al., 2020). Thermal re-equilibration to magmatic temperatures and hence to temperatures above the crystallographic stability of limestones ($T >$ ~850 °C for a Ca-rich limestone; Olszak-Humienik and Jablonski, 2015), are in the order of fractions of seconds to fractions of hours, depending on initial carbonate temperature and clast size. As an example, a 1 cm-radius spherical carbonate clast that is ingested in a magma at 1050 °C reaches 850 °C at the rim after some seconds and at the core in less than one minute, for a carbonate starting temperature of 300 °C (Buono et al., 2020). Experimentally, Escardino et al. (2008) found that thermal decomposition timescales of calcite powders (with particle sizes below 300 μm) decreased from 210 s to around 60 s after increasing the temperature from 850 °C to 950 °C.

Numerical models (Costa et al., 2007, 2009b; Massaro et al., 2018, 2019) have shown how the geometry of the feeding system of a volcano during an eruption is variable as a function of magma overpressure, elastic deformation of wall-rocks, and spalling and erosion around the fragmentation level. This dynamic behaviour is prone to favour wall rock entrapment into the ascending magma, triggering thermo-metamorphic reactions that may alter the eruptive dynamics. This is particularly true when the entrapped rocks are carbonates, whose thermo-metamorphism releases CO_2 as a volatile phase. CO_2 solubility at these shallow depths (i.e., $P < 0.2$ GPa) is extremely low for all kinds of magmas (e.g., Blank and Brooker, 1994; Thibault and Holloway, 1994; Lowenstern, 2001; Papale et al., 2006). Therefore, interactions of magma with shallow crustal carbonates promote the formation of a free CO_2 vapour phase since re-dissolution of CO_2 into the magma is highly unlikely at shallow crustal levels (Holloway and Blank, 1994; Troll et al., 2012a). Thus, in shallow *syn*-eruptive settings (i.e., $P < 0.2$ GPa and interaction timescales from seconds to tens of minutes), the focus needs to lie on the identification of decarbonation and clast dissolution rate of (ingested) carbonate wall-rocks, since the addition of volatile phases might ultimately increase eruption explosivity (Botcharnikov et al., 2005; Deegan et al., 2010). In nature the assimilation of wall-rocks will lead to a cooling of the magma, which induces (or accelerates) crystallization. If a magma reaches the critical crystal cargo fraction of ~50% it will not be able to further assimilate wall-rocks and/or magma ascent might cease. Glazner (2007) has described this thermal self-limiting effect of wall-rock assimilation in a study on granitic rocks which are entrapped in a basaltic magma. On the other hand, Carr et al. (2018), for example, found that adding as few as 1000 ppm of CO_2 to a portion of the magma at storage depth might be enough to cause local overpressurization of the magmatic mixture, which indicates that also low amounts of assimilated carbonate wall-rock might be sufficient to increase eruption explosivity. Numerical modelling of the effect of volatile phases on magma ascent dynamics of basaltic explosive eruptions shows that the addition of CO_2 from an external source (such as carbonate wall-rocks) and the resulting increase in the driving pressure causes a strong increase of mass eruption rate (La Spina et al., 2022). Despite the importance of *syn*-eruptive addition of volatiles via wall-rock decarbonation for eruption dynamics, a systematic investigation of decarbonation and clast dissolution timescales as well as their controlling parameters has not been conducted yet for extremely shallow or near-surface short-term magma carbonate interactions (i.e., at atmospheric pressure).

In this paper, we present such a systematic investigation on the influence of various parameters (including temperature, limestone, and magma composition) on syn-eruptive carbonate assimilation at atmospheric pressure, accounting for the upper endmember of the volcanic feeding system. While providing valuable insights in the carbonate assimilation process it needs to be noted that experiments at atmospheric pressure cannot reproduce pressure regimes experienced by natural samples during magma ascent. In previous studies a pressure representative of magma chamber levels (0.5 GPa = ~14 km depth) was applied, with the notable exception of Deegan et al. (2022) that did magma-shale (with a carbonate component) interaction experiments at 0.15 GPa. By comparing the results of all experimental approaches, we were able to qualitatively extrapolate the conditions and outcomes of magma carbonate interactions throughout the whole shallow volcanic feeding system, from magma chamber to Earth's surface. This enables a qualitative description of the syn-eruptive decarbonation of ingested carbonate-bearing wall-rocks and its controlling parameters throughout the whole volcanic feeding system and how this interaction within the feeding dyke of an eruption will influence the eruptive behaviour.

2. Methodology

2.1. Starting materials

The magma for most of the experiments was obtained from phonolitic grey pumice samples from the Pomici di Avellino eruption of Mt. Somma-Vesuvius without limestone xenolith content (EU3 base; Sulpizio et al., 2010). The samples were taken from the Traianello quarry (Somma-Vesuviana), denoted as Site B in Sulpizio et al. (2010). To evaluate the effect of magma composition on short-term magma-carbonate interaction, additional experiments with a basalt from the 2002 lava flow of Mt. Etna (Musu et al., 2021), and a shoshonite (K-rich basaltic andesite) from Vulcano Island (Italy; Vetere et al., 2007, 2011, 2013, 2015b; Pisello et al., 2022b) were conducted. These rocks were milled down to grain sizes lower than 200 μm at the Petro-Volcanology Research Group (PVRG) laboratory of the University of Perugia. The

powders were subsequently melted by utilizing a Nabertherm HT 04/17 furnace in air at supra-liquidus temperature (1400 °C). The melting time was set to 4 h, after which the melt was quenched to a glass (quenching rate was $>10^5$ K/h). Each glass was then re-crushed and milled and the melting-quenching procedure was repeated identically to obtain chemically homogeneous glasses (see Vetere et al., 2015a & Pisello et al., 2022a for further details on the glass preparation procedure).

Furthermore, to investigate the effect of limestone composition and texture, two Ca-rich limestones, a dense one (denoted C_d) and a microporous one (denoted C_{mp}), and a dolomitic (denoted D) limestone were used in the experiments (chemical compositions in Table 1). The dense Ca-rich limestone is from the Mesozoic carbonate relieves east of Somma-Vesuvius (Scandone et al., 1991). The microporous Ca-rich limestone is of the Scaglia Bianca Formation near Furlo (Central Apennines, Italy; Cosentino et al., 2010). The Mg-rich dolomitic limestone is from the Apulian carbonate platform near Polignano a Mare (Puglia, Southern Italy; Andriani and Walsh, 2007). While both Ca-rich limestones are macroscopically and microscopically homogeneous, the dolomitic limestone is heterogeneous (lighter and darker areas) and has even some fractures filled with calcite crystals (Fig. 1). For the experiments, the limestone clasts were cut into square cuboidal pieces (ca. 5 mm x ca. 5 mm x ca. 10 mm), corresponding to a weight of 0.7–1.0 g. We will refer to them as "large" clast size (LC). To investigate the effect of a smaller clast size (and therefore larger surface to volume ratio), some samples were cut in smaller cubic pieces (ca. 5 mm x ca. 5 mm x ca. 5 mm), corresponding to a weight of 0.4–0.7 g, which will be referred to as "small" clast size (SC).

The whole rock chemical composition for all starting materials is derived by X-ray fluorescence (XRF) analysis at the Department of Earth and Geoenvironmental Sciences of the University of Bari and is given in Table 1.

Despite the differences in texture and composition the theoretical maximum of volatile phases (mainly CO_2) that can be released (in wt%) from all three limestones is similar: for the dense Ca-rich limestone it is 43.73%; for the microporous Ca-rich limestone 43.38%; for the dolomitic limestone 46.60% (Table 1).

2.2. Experimental procedure

The experiments are designed to represent *syn*-eruptive magma carbonate interactions at the upper endmember of the volcanic feeding system. Therefore, we chose a relatively simple experimental set-up, in which the limestone clasts were ingested into a melt at atmospheric pressure in open ceramic crucibles (Al_2O_3-crucibles). The experiments were performed in a Nabertherm HT 04/17 furnace at the Department of Physics and Geology at the University of Perugia and the experimental procedure was carried out in the following steps:

(1) The ceramic crucibles were weighed empty and filled with 7–8 g of the pre-prepared dry glasses from the starting materials. The limestone clasts were weighed and assigned to a distinct ceramic crucible (Fig. 2A). The combined weight of glass shards, ceramic crucible and limestone clast is noted.
(2) The ceramic crucible with the glass shards was heated in the furnace up to 1400 °C and remained there for around 30 min to melt the glass and remove any residual amounts of H_2O or other volatiles (visible bubbles). Afterwards it was quenched at room temperature (to prevent crystals to form) and weighed again (Fig. 2B). If the weight of ceramic crucible and glass differs from the weight before, we repeated this step until the weight stayed the same (± 0.002 g).
(3) After this initial check, we started the experimental procedure, by putting the ceramic crucibles (with the glass inside) into the furnace at 1230 °C. The crucibles were left there for 15–20 min to guarantee an equal distribution of temperature throughout the whole sample.
(4) The ceramic crucible was removed from the furnace and placed on heat resistance plate. The limestone clasts (previously weighed) were pushed into the melt with a pair of pliers (Fig. 2C). This step needs to be performed as quick as possible to prevent an increase in viscosity of the melt which makes it impossible to push the clast in.
(5) After pushing the limestone clast into the melt, the samples were quenched at room temperature and weighed again (Fig. 2D). The weight loss measured now, called initial weight loss, is due to the limestone clast already decomposing and releasing some CO_2 (Table 3). Since clast ingestion at 950 °C is not feasible due to the high melt viscosity, we inserted the carbonate clast for all samples at 1230 °C. After insertion, we quenched them, subtracted the initial weight loss from the whole CO_2 budget, and then conducted the experimental runs in the furnace at the experimental temperature. In this way, the experiments at 950 °C and 1230 °C are comparable. The initial weight loss is noted but not regarded in the following analysis. For the analysis we considered only the weight loss from the experimental runs (Step 6).
(6) The experimental runs: the furnace is set to the experimental temperature (950 °C or 1230 °C). After at least 15 min at this temperature, we put the cold ceramic crucible (with glass and carbonate clast inside) into the furnace for the planned experimental duration (60–1800 s). The opening of the furnace door causes a small temperature drop and the experimental dwell time is counted only after re-equilibrating to the experimental temperature (in our case: ~25 s for the 1230 °C runs and ~ 5 s for the 950 °C runs).
(7) As soon as the experimental runtime expired, the samples were taken out of the furnace and rapidly quenched at room temperature to prevent crystal formation (Fig. 2E).
(8) After cooling to room temperature, the samples are weighed again (Fig. 2F). The measured weight is subtracted from the measured weight after clast ingestion (i.e., after Step 5) to account only for the weight loss that occurred during the experimental run. This weight loss of the experimental run was then compared to the weight of the CO_2 still present in the limestone

Table 1
Chemical compositions (in wt%) of the starting materials derived by XRF - Analysis. *) total iron content: FeO(tot) = Fe_2O_3 + FeO, **) LOI = loss of ignition: volatile content of material (here: mainly CO_2 content in limestones), ***) melt viscosities at 1230 °C (and 950 °C for VP) derived via the model of Giordano et al. (2008).

Chemical compositions of Limestones and Glasses													
	SiO_2	TiO_2	Al_2O_3	FeO (tot)*	MnO	MgO	CaO	Na_2O	K_2O	P_2O_5	LOI**	Total	log $\eta_{1230°C}$ [Pa*s]***
Dolomitic Limestone (D)	0.15	0.00	0.08	0.06	0.00	18.78	34.32	0.00	0.01	0.00	46.60	100.00	–
Ca-rich Limestone (C_d)	0.20	0.00	0.08	0.03	0.00	0.44	55.46	0.02	0.02	0.00	43.73	99.98	–
Ca-rich Limestone (C_{mp})	0.84	0.01	0.22	0.13	0.03	0.46	54.82	0.02	0.11	0.00	43.38	100.02	–
											VP log $\eta_{950°C}$:		6.82
Vesuvius Phonolite (VP)	55.63	0.31	21.85	3.07	0.00	0.09	4.46	5.57	8.23	0.00	–	99.21	3.85
Vulcano Shoshonite (VS)	53.33	0.65	15.29	7.63	0.16	4.15	7.76	5.08	3.04	0.50	–	97.59	2.34
Etna Basalt (EB)	47.70	1.70	16.15	10.18	0.18	6.27	10.77	3.39	1.95	0.52	–	98.81	1.55

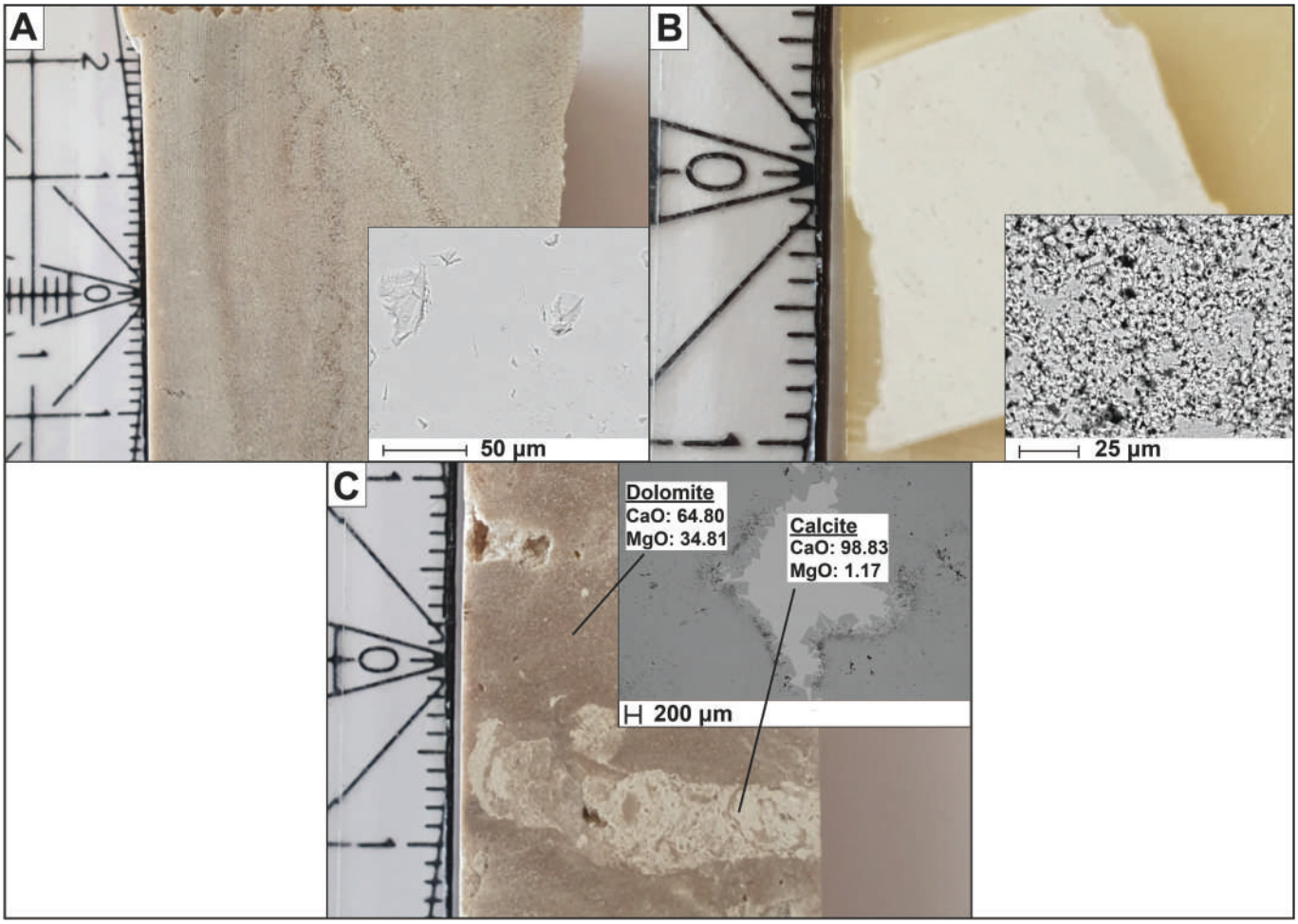

Fig. 1. Comparison of the three different types of limestone used in the experiments: A) a dense Ca-rich limestone, texture (macroscopically and microscopically) and chemistry homogeneous, B) a microporous Ca-rich limestone, texture is macroscopically homogeneous but microscopically porous, chemistry is homogeneous, and C) a dolomitic limestone, texture is both macroscopically and microscopically heterogeneous and comprised of darker dolomitic areas (CaO vs. MgO = 65 to 35 wt%) and lighter Ca-rich areas (CaO vs. MgO = 99 to 1 wt%). The macroscopic images have a scale to their left, where 0–1 equals one centimetre. The microscopic images are SEM BSD images with the scale at the bottom of each picture. The CaO and MgO content (in Fig. 1C) is derived by Energy Dispersive Spectrometry (EDS) point analysis (conducted at the Department of Earth and Geoenvironmental Sciences of the University of Bari, Italy).

clast (i.e., the weight loss from Step 5 has been subtracted). Finally, we normalised the weight loss percentage to a value between 0 and 1, where 1 implies that 100% of the CO_2 (i.e., the amount of CO_2 left in the limestone after Step 5) was lost. Only these weight loss values were considered in the further analysis within this study.

Each experimental series (i.e., a set of experiments with a distinct combination of fixed experimental parameters) consisted of 7 experiments varying in experimental runtime (t = 0, 60, 150, 300, 600, 1200 and 1800 s).

Due to the (partial or complete) thermal decomposition of the carbonates (i.e., the release of CO_2), the relicts consist now mainly of CaO (and MgO in the case of dolomitic starting material). CaO and MgO are hygroscopic; therefore, the samples need very careful handling after the experiments, not exposing them to any water or humidity. Thus, the samples were inserted in a resin to preserve the *status quo* until the preparation for the scanning electron microscopy (SEM) analysis, for which a crosscut with a polished surface needed to be prepared.

2.2.1. *Limitations of the experimental procedure*

It needs to be pointed out that while this experimental procedure has its advantages for observing the decarbonation process very directly, it also has several limitations. These limitations regard mainly: i) the absence of water content in our melts, ii) the isothermal nature of our experiments and, iii) the insertion of cold experimental samples for the experimental run and the subsequently needed re-heating process of the experimental sample to the experimental temperature (i.e., Steps 5 and 6 of the experimental procedure).

Most importantly, since we used open crucibles to measure the decarbonation directly via weight loss of our experimental samples, we could only use dry melts in our experiments. The absence of water in our melts will slow down the clast dissolution process, as the diffusion of almost all major elements (including Ca and Mg) is strongly enhanced by the presence of H_2O in the melt (Zhang et al., 2010; González-García et al., 2017). Thus, we would need to expect slowed down clast dissolution in our experiments with dry melts.

The second limitation regards the application of our results to natural systems, as we conducted isothermal experiments. Given the low temperature of wall-rocks during ingestion (100–500 °C; Sottili et al., 2010) in nature the assimilation of wall-rocks will consume energy (i.e., in form of heat) and effectively cool down the magma temperature, inducing crystallization which leads to an increase in magma viscosity. If the magma reaches the critical solid fraction of ~50% it undergoes a transition from a viscous liquid to a semi-rigid crystal network (Costa, 2005; Glazner, 2007; Costa et al., 2009a), which ultimately causes

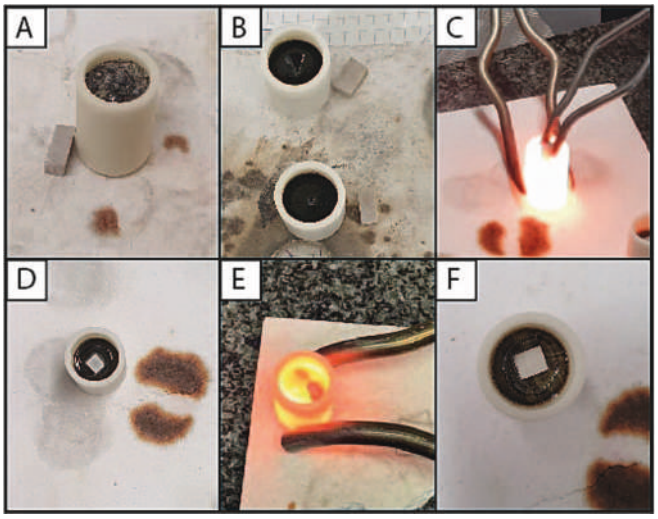

Fig. 2. The experimental procedure depicted in six main steps: A) The starting materials: dry glass shards in the ceramic crucible and the limestone clast, B) Uniform glass in the ceramic crucible after the first melting step, C) insertion of the carbonate clast into the melt, D) cooling the sample to room temperature and subsequent weighing of initial CO_2 loss, E) putting sample back in the oven for experimental runs and F) final cooling of a sample after the experiment and final weighing for total CO_2 loss of sample. The inner diameter of the ceramic crucible is 16 mm.

magma ascent to cease. This self-limiting effect of wall-rock assimilation has previously been described by Glazner (2007) for granitic wall-rocks (with a $T_{wall\text{-}rock}$ = 400 °C) being entrained into a basaltic melt at 1125 °C, where 25% of granite are enough to cause the transition to a semi-rigid crystal network. To make our results applicable to nature we must be aware that we cannot assimilate infinite amounts of crustal material. Hence, in nature CO_2 release and clast dissolution might cease during extensive crustal assimilation.

The third limitation is connected to the quenching of the samples after inserting the limestone clasts to make the experiments at high and low temperature comparable (i.e., Step 5 of experimental procedure). For the experimental runs, we then proceeded to put the cold samples back in the oven, which was pre-heated to the experimental temperature (i.e., Step 6 of experimental procedure). In Fig. 3 we show the results of two approaches to determine the time for thermal re-equilibration of the sample to the experimental temperature.

The first approach, the so-called lumped system analysis ("x"-curves), is a simplified theoretical approach in which the interior temperature of a body (here the alumina crucible) is assumed to remain uniform during heat transfer. The time needed to heat an object can then be calculated via the following equation:

$$t = \left(\left(m^* c_p\right)/\left(A^* h\right)\right)^* ln\left(\left(T_0 - T_{exp}\right)/\left(T_1 - T_{exp}\right)\right) \quad (1)$$

in which m is the mass, c_p is the specific heat and A the surface area of the ceramic crucible (only considering the outer surface), h is the heat transfer coefficient, T_0 is the Temperature of the ceramic crucible before inserting it in the oven, T_1 is the temperature the crucible should be heated to and T_{exp} is the temperature the oven is set to. The values for all variables are given in Table 2.

The second approach was to measure the temperature directly with a thermocouple on top of the experimental sample (dotted curves). With this approach we could not measure with certainty the ceramic crucible but more likely measured the temperature of the air in its immediate surrounding (Fig. 3b). Therefore, the first approach can be seen as

Table 2
Parameters for lumped system analysis. *) Specific heat is taken from the material data sheet of the crucibles (Degussit AL23 of KYOCERA Fineceramics Solutions GmbH), **) Heat transfer coefficient between air and alumina crucible is T-dependent. Here we used the mean value calculated by Andersen et al. (2015) in the T interval 100–750 °C, ***) Since we cannot divide by zero in eq. (1) T_{exp} needed to be set to a slightly higher value.

Parameters for lumped system analysis							
mass of ceramic crucible	m	0.0145	kg	starting T of crucible	T_0	20	°C
specific heat of crucible *	c_p	900	J/kg*K	T crucible needs to be heated to	T_1	950 / 1230	°C
outer surface area of crucible	A	0.004411	m^2	T oven is set to ***	T_{exp}	951 / 1231	°C
heat transfer coefficient **	h	265	W/m^2*K				

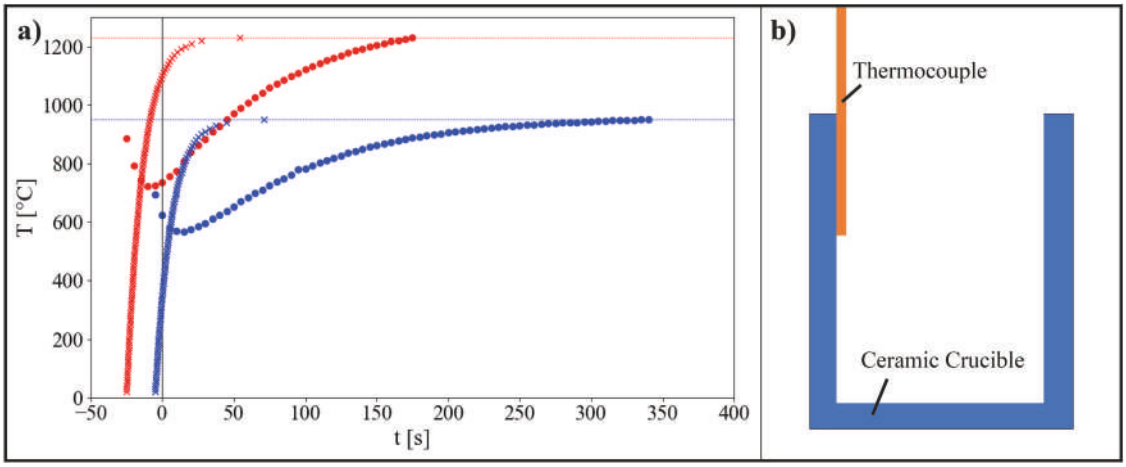

Fig. 3. *Re*-heating of the experimental sample: a) two approaches to calculate the time the exp. sample needs to re-equilibrate to the temperature of the oven (950 °C in blue and 1230 °C in red): "x"-curves are values derived via the lumped system analysis and the dotted curves are derived via measurements with a thermocouple in the direct vicinity of the ceramic crucible. Time "0 s" here corresponds to when we started the experimental runtime (i.e., when the temperature within the oven was back at the experimental temperature after inserting the sample: ~25 s at 1230 °C and ~ 5 s at 950 °C (see Step 6 of experimental procedure)), while the re-heating of the sample was calculated/measured directly after inserting them in the oven (hence the negative starting times). b) schematic figure of the thermocouple approach. (For interpretation of the references to colour in this figure legend, the reader is referred to the web version of this article.)

optimistic, while the second one should be closer to the real conditions.

Lastly, this experimental set-up does not allow for controlling the oxygen fugacity.

2.3. Calculation of decarbonation timescale (τ)

Since we used dry magmas and open crucibles, we could ascribe the weight loss to the CO_2 that left the limestone sample. For all three types of limestones used in the experiments, the amount of CO_2 theoretically present in every clast was determined via XRF-analysis, during which the loss on ignition (i.e., the weight loss due to heating and subsequent volatile release) was measured (Table 1). As explained in the methodology section, there is an initial weight loss after inserting the limestone clasts into the magma. This initial loss is not regarded in the analysis but is nevertheless given for each series in Table 3. Consequently, the initial loss is subtracted from the theoretically available CO_2 budget (as derived from XRF-analysis) and not considered in the results (Figs. 4–7). The remaining CO_2 budget (after Step 5) was normalised to the maximum loss of CO_2, where 1 indicates 100% loss. Each experimental series consisted of 7 experiments at varying experimental duration (0–1800 s). In Figs. 4–7, we plotted the CO_2 loss fraction vs. the experimental runtime. The datapoints were fitted using a simple one-parameter sigmoidal function such as:

$$F(t) = erf\ (t/\tau) \quad (2)$$

in which *erf* is the error function, t is the experimental runtime (in seconds) and τ is the characteristic timescale of decarbonation (in seconds). The fitting equation is shown as a red dotted line within the plot of each series. The r^2-value gives the goodness of the fit and is above 0.9 in all experimental runs (Figs. 4–7). In order to account for the variability of the experimental data, we considered a 10% confidence interval around the fitted line to account for the experimental errors (e.g., small residual amounts of H_2O in magma, bubble bursts that ejected small amounts of material out of the crucible, inhomogeneities in the limestone clasts and hence small deviations from the LOI or simple weighing inaccuracies).

2.4. Analytical methods (SEM)

Scanning Electron Microscopy (SEM) images and data were acquired in the Department of Earth Geoenvironmental Sciences of the University of Bari using a SEM (LEO EVO-50XVP Zeiss, Cambridge, UK) coupled with an energy dispersive X-ray spectrometer (EDS; Oxford-Link Ge ISIS equipped with a SuperAtmosphere Thin Window©) for qualitative X-ray detection.

The SEM investigation was carried out on polished and graphite-coated cross-sectional cuts of the experimental samples by counting Back Scattered Electrons (BSE). The parameters selected to perform the analysis were: 15 kV accelerating potential, 500 pA probe current and 20 s counting time. For elemental composition analysis and chemical mapping, X-ray intensities obtained by the EDS spectrometer were converted to wt% of oxides by the ZAF4/FLS quantitative analysis software of Oxford-Link Analytical (UK). The accuracy of the analytical data was checked through standard minerals manufactured by Micro-Analysis Consultants Ltd. (UK). Analytical precision was 0.5% for concentrations >15 wt%, 1% for concentrations of about 5 wt% and < 20% for concentrations near the detection limit, which depends on the considered element, but it is never below 1000 ppm (Caggiani et al., 2015).

For the SEM analysis, the samples were cut at the same height (~ the half). We chose to do the diffusion analysis from centre of the (ex-) limestone clast to the rims (i.e., towards the sides not the corners) and around 1 mm into the glass. The analysis along this line was conducted within small areas (to minimize eventual errors compared to point measurements) with a width of 30 μm (and height of 150 μm), and some (3–5) smaller areas directly at the glass – carbonate contact (same height, width of 10 μm). All samples (besides the 1200s-sample) of the VP01 experimental series (i.e., phonolitic melt, 1230 °C, dolomitic limestone and "large" clast size, Table 3) were chosen for the diffusion analysis to have a diffusion analysis over the whole range of experimental runtimes for one series. To check the influence of melt composition and temperature on clast dissolution via diffusive transport of Ca and Mg from the limestone clast into the melt, we selected two samples (300 s and 1800 s) of the high temperature experimental series with basalt and ingested dolomitic limestone (EB02 series) and two samples of the low temperature (950 °C) experimental series with phonolitic melt and ingested dolomitic limestone (VP04 series).

3. Results

As indicated in the introduction, we divided the results of our carbonate assimilation experiments into the observable and quantifiable sub-processes, namely limestone decarbonation and clast dissolution, following the nomenclature introduced by Knuever et al. (2022). Throughout the experimental sessions, we varied important parameters like temperature, limestone composition, magma composition, clast size and limestone texture. We conducted experiments with various combinations of these parameters to identify the influence of the single parameter on the timescales of limestone decarbonation and clast dissolution in carbonate assimilation at atmospheric pressure. The experimental results are summarized in Table 3.

3.1. Limestone decarbonation

During the first experimental runs, we tested the effect of temperature and limestone composition (Fig. 4) at constant magma composition

Table 3
Table of all experimental series and their parameters. Each series comprises 7 experiments at increasing runtimes (0–1800 s) except for the porous Ca-rich limestone series, where the 1500 s experiment is missing. S/V: gives the surface to volume ratio and "large" clast size equals to a S/V of 9 mm^{-1} and "small" clast size equals to S/V of 11.33 mm^{-1}; T: gives the experimental temperature in this series; Initial loss of CO_2: gives the loss of CO_2 (in wt%) after inserting the carbonate clast into the melt but before the experiment (i.e., after Step 5); τ: gives the characteristic timescale (in s) of the decarbonation process for each series; W_D: gives the width (in μm) of the diffusion-affected area around the ingested limestone clast.

Exp. series number	Type of magma	Type of limestone	S/V [mm^{-1}]	T	Initial Loss of CO_2	τ [s]	W_D after 300 s [μm]	W_D after 1800 s [μm]
VP01	VP	Ca-rich	9	1230 °C	4%	232	–	–
VP02	VP	dolomitic	9	1230 °C	32%	143	160	390
VP03	VP	Ca-rich	9	950 °C	5%	999	–	–
VP04	VP	dolomitic	9	950 °C	33%	626	0	30
VP05	VP	dolomitic	11.33	1230 °C	40%	155	–	–
VP06	VP	dolomitic	11.33	950 °C	40%	643	–	–
VP07	VP	microporous Ca-rich	9	1230 °C	14%	219	–	–
VS01	VS	Ca-rich	9	1230 °C	7%	245	–	–
VS02	VS	dolomitic	9	1230 °C	37%	165	–	–
EB01	EB	Ca-rich	9	1230 °C	8%	247	–	–
EB02	EB	dolomitic	9	1230 °C	35%	163	200	680

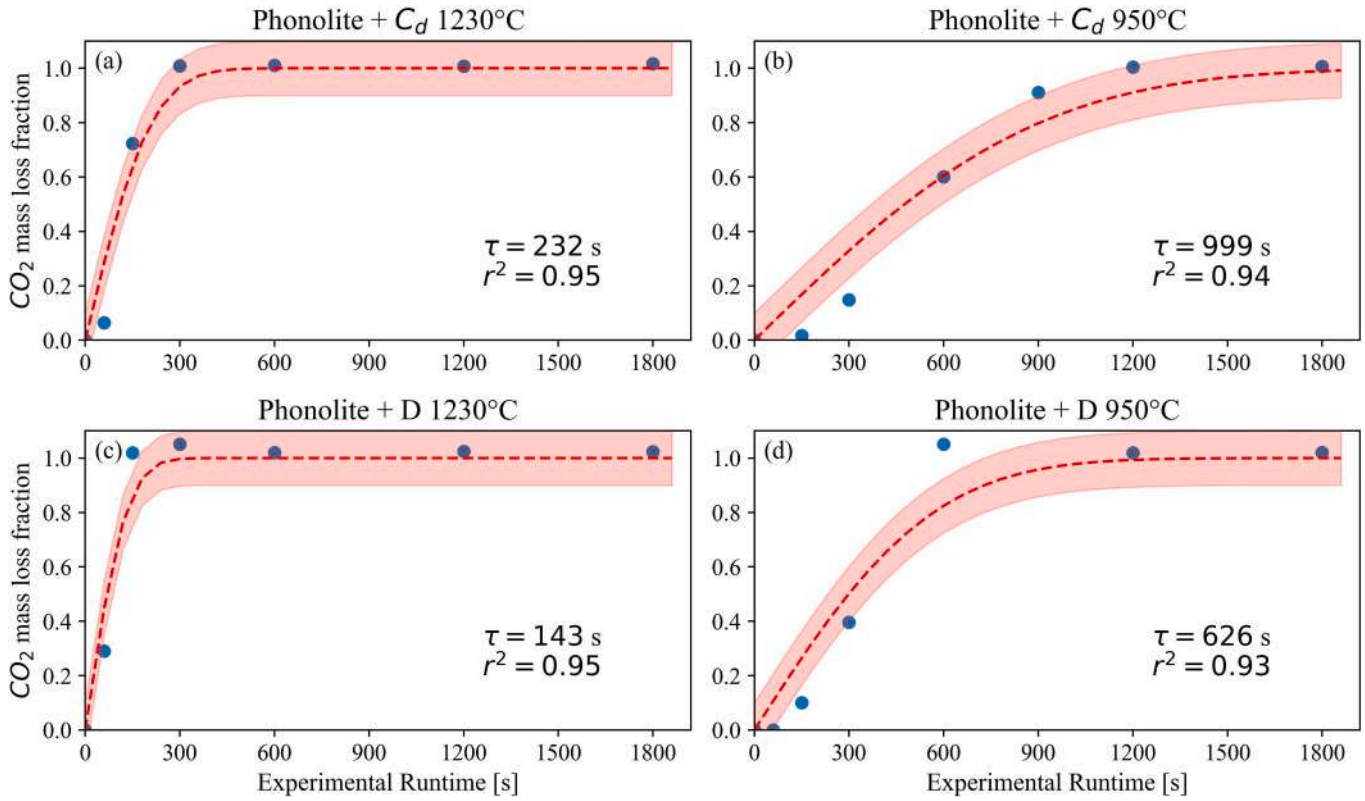

Fig. 4. CO_2 mass loss fraction versus experimental runtime. On the y-axis, a value of 1 describes the maximum theoretical CO_2 loss of the remaining CO_2 (i.e., after the subtraction of initial loss (see Table 3)). In the graphs above we tested the influence of temperature (1230 °C in Fig. 4 a&c vs. 950 °C in Fig. 4 b&d) and the influence of limestone composition (dense Ca-rich in Fig. 4 a&b vs. dolomitic in Fig. 4 c&d). τ gives the characteristic timescale of decarbonation for each series derived from the fitted curve and the r^2-value the goodness of the fit.

(Somma-Vesuvius Phonolite) and clast size. For both high-temperature series, the characteristic timescale of decarbonation (τ) is below 240 s (down to 140 s), while in both low temperature series, the value of τ is above 600 s (up to 1000 s, or 16.6 min). It can also be seen that for both series with dolomitic limestones the values of τ are lower (143 s at 1230 °C and 626 s at 950 °C) than for the series with Ca-rich limestone (232 s at 1230 °C and 999 s at 950 °C).

To test the effect of magma composition and hence magma viscosity on CO_2 release, we ran the same experiments at high temperature (1230 °C) with a basalt from Etna and a shoshonite from Vulcano (Eolian Islands, Italy). A comparison of the magma compositions and their respective viscosities at 1230 °C (by using the model of Giordano et al., 2008) is given in Table 1. The experiments were carried out with both Ca-rich and dolomitic limestone clasts. The characteristic timescale of decarbonation (τ) varies only little with the three different magma compositions and is in the range of 230–250 s for the experiments with the dense Ca-rich limestone and in the range of 140–170 s for the dolomitic limestone (Fig. 5).

The effect of the clast size on the decarbonation timescale was tested with the same experimental set-up at high (1230 °C) and low temperature (950 °C) and by using phonolite from Vesuvius. The decrease in clast size resulted in an increase in surface to volume ratio of about 25%. In the high-temperature experiments (Fig. 6 a&b), the values of τ are almost equivalent (143 s for the "large" clast size and 155 s for "small" clast size). Likewise, in the low-temperature experiments (Fig. 6 c&d), they are very similar (626 s for the "large" clast size and 643 s for the "small" clast size). It needs to be mentioned that the initial loss of CO_2 (which is disregarded within the diagrams) increases slightly with increasing surface to volume ratio (i.e., for the "smaller" clasts; Table 3).

Lastly, the influence of limestone texture was tested with the same experimental set-up and at a temperature of 1230 °C. We used two Ca-rich limestones in these experiments, a dense one and a microporous one. For the dense Ca-rich limestone, the value of τ is 232 s and for the microporous one τ equals 219 s (Fig. 7 a&b, respectively).

3.2. *Clast dissolution*

A complete dissolution of the ingested carbonate clast was not observed in any of the experiments, not even in the longest lasting experiments (Figs. 8 & 9). The analysis of the extent of diffusive transport of Ca (and Mg in the case of dolomitic limestones) from the ingested limestone clast was conducted exemplarily for the whole VP02 experimental series (phonolitic melt and dolomitic limestones at 1230 °C) and then compared to selected experiments of the VP04 (phonolitic melt and dolomitic limestones at 950 °C) and EB02 experimental series (basaltic melt and dolomitic limestones at 1230 °C). The phonolitic starting melt contains about 4.5 wt% CaO and around 0.1 wt% MgO, while the basaltic starting melt contains around 10.8 wt% CaO and 6.3 wt% MgO (Table 1). Note that the varying concentrations of Ca and Mg in the dolomitic clast are due to its heterogeneous nature, hosting even pure calcite veins (Fig. 1). Hence, we decided to show the concentration plots once with Ca and Mg concentrations separated and once combined.

The onset of Ca and Mg diffusion from the ingested clast into the phonolitic melt lies between the 150 s- and 300 s-experiment. In the 300 s-experiments an increase in Ca and Mg in the glass due to diffusion is measurable in a ~ 160 μm wide area. The width of the diffusion affected area increases with experimental runtime to ~280 μm in the 600 s-experiment and to its maximum width of ~390 μm in the 1800s-experiment.

Furthermore, to test effect of melt composition on the diffusion (or clast dissolution) two samples of the experimental series with basaltic melt, in which "large" sized dolomitic limestones were ingested at

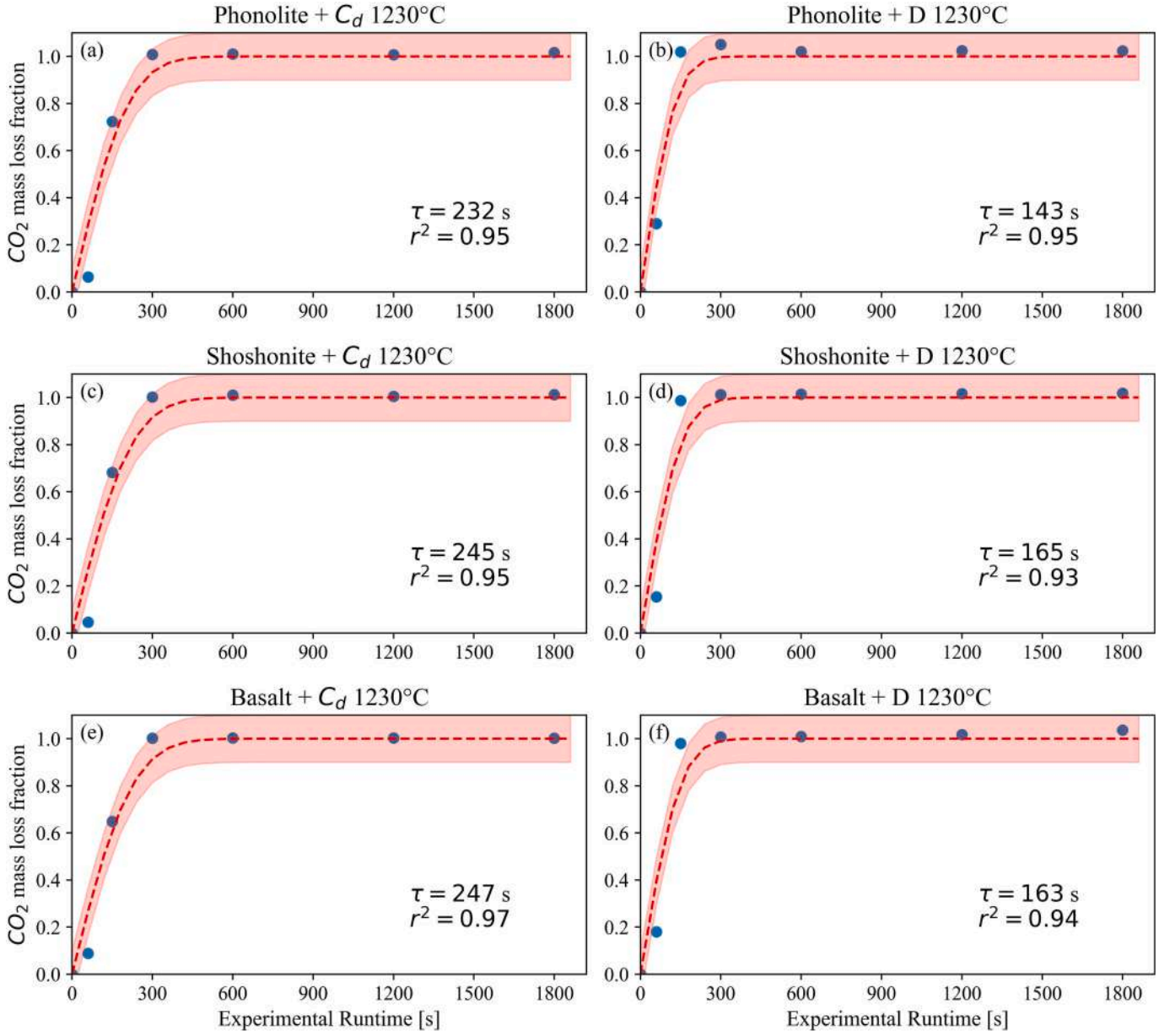

Fig. 5. CO_2 mass loss fraction versus experimental runtime. On the y-axis, a value of 1 describes the maximum theoretical CO_2 loss of the remaining CO_2 (i.e., after the subtraction of initial loss (see Table 3)). Three different magmas were used to test the influence of magma composition and hence viscosity: Vesuvius Phonolite (Fig. 5 a&b), Vulcano Shoshonite (Fig. 5 c&d) and Etna Basalt (Fig. 5 e&f). τ gives the characteristic timescale of decarbonation for each series derived from the fitted curve and the r^2-value the goodness of the fit.

1230 °C were analysed. The choice for the 300 s- and 1800s-experiments of this series is due to it being the onset and the maximum extent of diffusion into the glass in the phonolitic series. Note that, both high temperature experimental series show the same timescale for decarbonation (~150 s, Fig. 5), while the decarbonation in the low temperature experiments required more time (~630 s, Fig. 4).

Ca and Mg diffusion from the ingested dolomitic clast into the phonolitic melt at 950 °C is absent in almost all our experiments (Fig. 9 a&b); only in the longest lasting run (1800 s) a very slight increase in Ca is measurable in the first 30 μm of the glass directly at the glass – carbonate interface. The decrease in Ca and Mg in the 1800s-experiment within the dolomitic clast near the interface is due to a relative increase in sulphur-concentration (up to 15 oxide wt%) and not due to decreases in Ca or Mg concentrations. The widths of the diffusion-affected areas around the ingested dolomitic clast in basaltic melts are ~200 μm and ~ 680 μm (for experimental durations of 300 and 1800 s, respectively; Fig. 9 c&d).

4. Discussion

The experiments, conducted at atmospheric pressure and in open ceramic crucibles, are designed to be the opposite endmember to the existing short-term carbonate assimilation studies that were conducted at p-T conditions of the magma chamber or below (1200 °C, 0.5–1 GPa; Deegan et al., 2010; Jolis et al., 2013; Blythe et al., 2015). Their main results are summarized in Table 4.

As discussed in Knuever et al. (2022), carbonate assimilation is not a single process, but a combination of several physical and chemical processes. Conversely to previous studies, we focused on the *syn*-eruptive and hence short-term (timescale of minutes) decarbonation of ingested limestone clasts at the second endmember of the volcanic feeding system and thus conducted the experiments at atmospheric

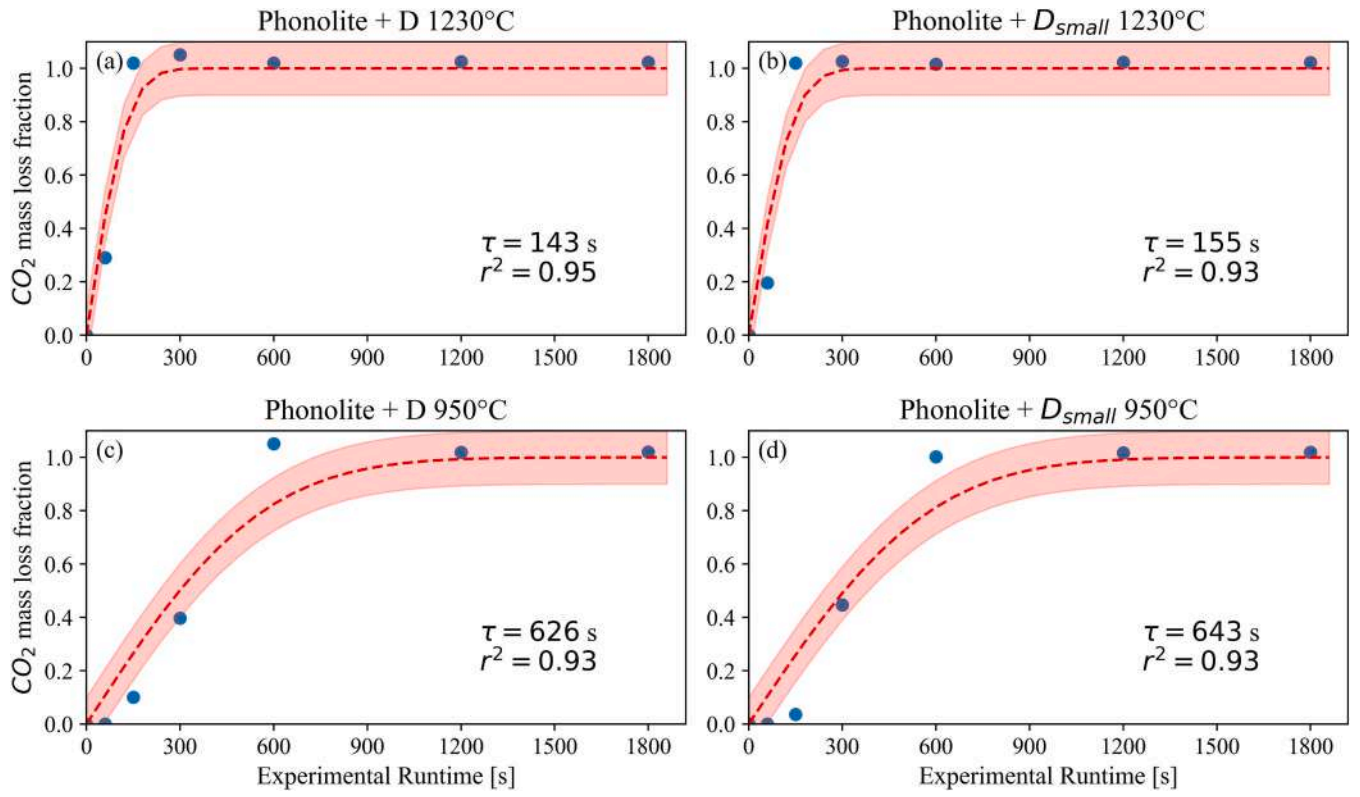

Fig. 6. CO_2 mass loss fraction versus experimental runtime. On the y-axis, a value of 1 describes the maximum theoretical CO_2 loss of the remaining CO_2 (i.e., after the subtraction of initial loss (see Table 3)). Here we compare two different initial clast sizes, resulting in different surface to volume ratios: Fig. 6 a&c are "large" sized (s/v = 9 mm^{-1}), Fig. 6 b&d are "small" sized (s/v = 11,33 mm^{-1}). τ gives the characteristic timescale of decarbonation for each series derived from the fitted curve and the r^2 -value the goodness of the fit.

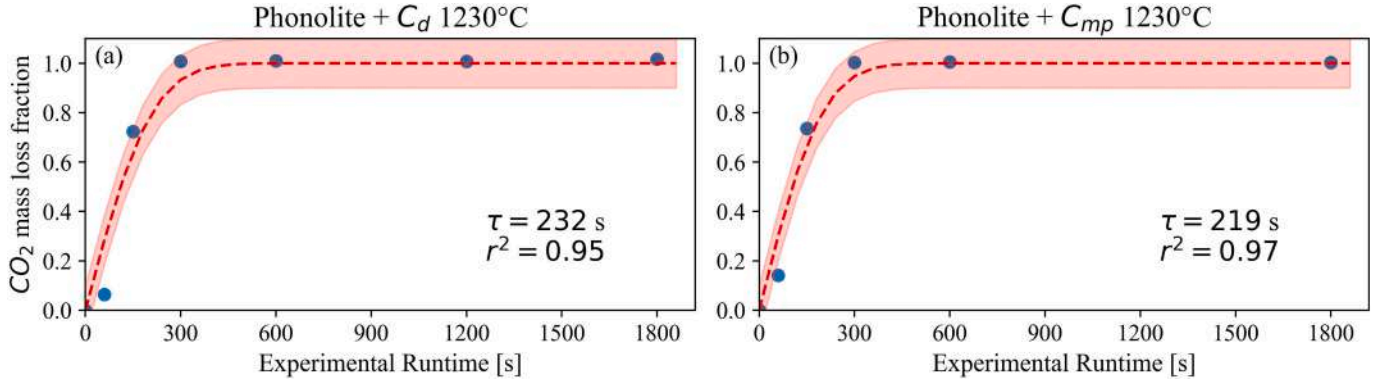

Fig. 7. CO_2 mass loss fraction versus experimental runtime. On the y-axis, a value of 1 describes the maximum theoretical CO_2 loss of the remaining CO_2 (i.e., after the subtraction of initial loss (see Table 3)). Above we compare the effect of different limestone textures: a) dense and b) microporous Ca-rich limestone. τ gives the characteristic timescale of decarbonation for each series derived from the fitted curve and the r^2 -value the goodness of the fit.

pressure. Within this study, a broad range of parameters has been varied to identify their influence on the characteristic decarbonation timescale (τ), including temperature, limestone composition, magma composition (and hence magma viscosity), and the size (i.e., surface to volume ratio) of the ingested limestone clasts. In addition, some new findings on the dissolution process have been obtained, which due to the experimental set-up might be valid only in a very limited range of cases.

The characteristic timescale of decarbonation (τ) was found to be mainly dependent on temperature and limestone composition (Fig. 4), with temperature causing the most pronounced difference of around factor 4.2–4.4 (between 950 °C and 1230 °C). The difference between Ca-rich and dolomitic limestone is not as pronounced but still significant and accounts for a factor of 1.5–1.6 in our experiments (Fig. 4). Furthermore, τ seems to be independent of or only slightly dependent on melt composition (Fig. 5) and limestone texture (Fig. 7) and, in our experiments, also clast size (Fig. 6). Our results are in agreement with previous decarbonation studies performed by Escardino et al. (2008) who have demonstrated the temperature dependence of the decarbonation rate already in experiments with calcite powders (without interaction with a magmatic body). Furthermore, the syn-eruptive nature of the timescale of decarbonation (seconds to several minutes) is in agreement with previous experimental carbonate assimilation studies at deeper conditions (0.5 GPa; Deegan et al., 2010; Jolis et al., 2013; Blythe et al., 2015) and thermal re-equilibration modelling (Sottili et al., 2010; Freda et al., 2011; Buono et al., 2020; Carr et al., 2020). Conversely to our results, clast size is a parameter significantly impacting the timescale

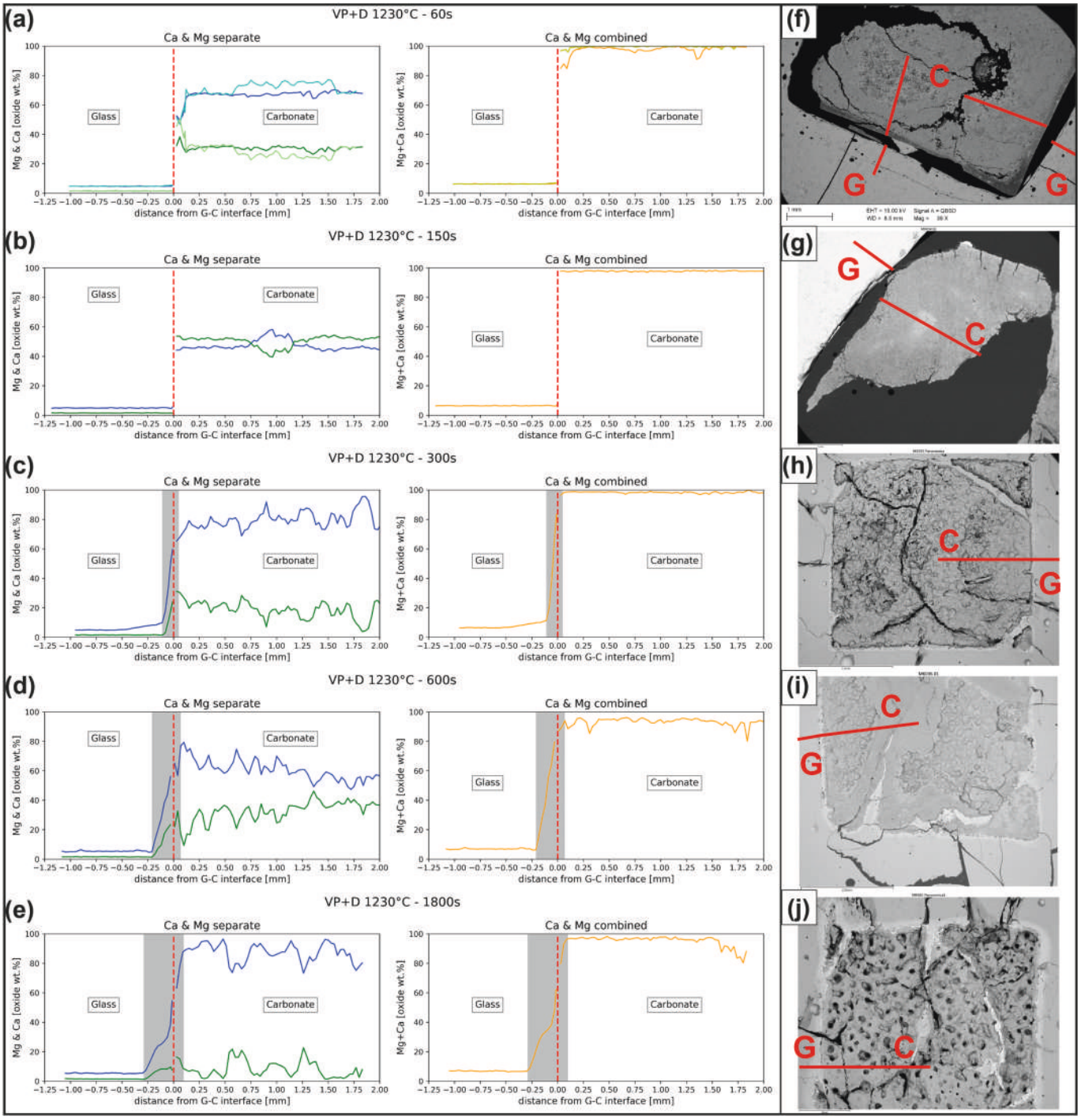

Fig. 8. Diffusion profiles of Ca & Mg in our experimental samples of the VP02 series (1230 °C, phonolitic melt, dolomitic limestone, "large" sized clast). Fig. 8 a-e shows the profiles with increasing interaction time (from 60 to 1800 s). The y-axis gives the Ca- and Mg-concentrations in weight % of the oxides, on the x-axis the distance from the glass-carbonate interface (red-dotted line) is given in mm. The green lines correspond to Mg-concentration, the blue lines to Ca-concentration and yellow line to combined Ca + Mg-concentrations. The diffusion-affected areas are highlighted as the grey areas. Note that the variable Ca- and Mg-concentrations are due to the heterogeneous nature of the dolomitic clast (as shown in Fig. 1). Fig. 8 f-j are the corresponding SEM-images in which the carbonate (C), the glass (G) and the lines corresponding to the diffusion measurement are given (red lines). The line within the carbonate is in between 1.8 and 2.1 mm in length, the line in the glass around 1 mm. (For interpretation of the references to colour in this figure legend, the reader is referred to the web version of this article.)

of thermal re-equilibration (Sottili et al., 2010; Freda et al., 2011; Buono et al., 2020; Carr et al., 2020). A possible explanation for this discrepancy could be that despite changing the surface-to-volume ratio from the "large" to the "small" clasts in our experiments, the "radius of the shortest axis" (i.e., the shortest line from the centre of the clast to one of its sides) did not change, since the minimum thickness remained unchanged (~5 mm). Hence, the change of clast size did not affect the decarbonation timescale in our experiments since the distance for thermal re-equilibaration remains the same for both clast sizes. In general, clast size should be considered a significant factor, as shown in previous studies (Sottili et al., 2010; Freda et al., 2011; Buono et al., 2020; Carr et al., 2020). We speculate that the dependence on limestone

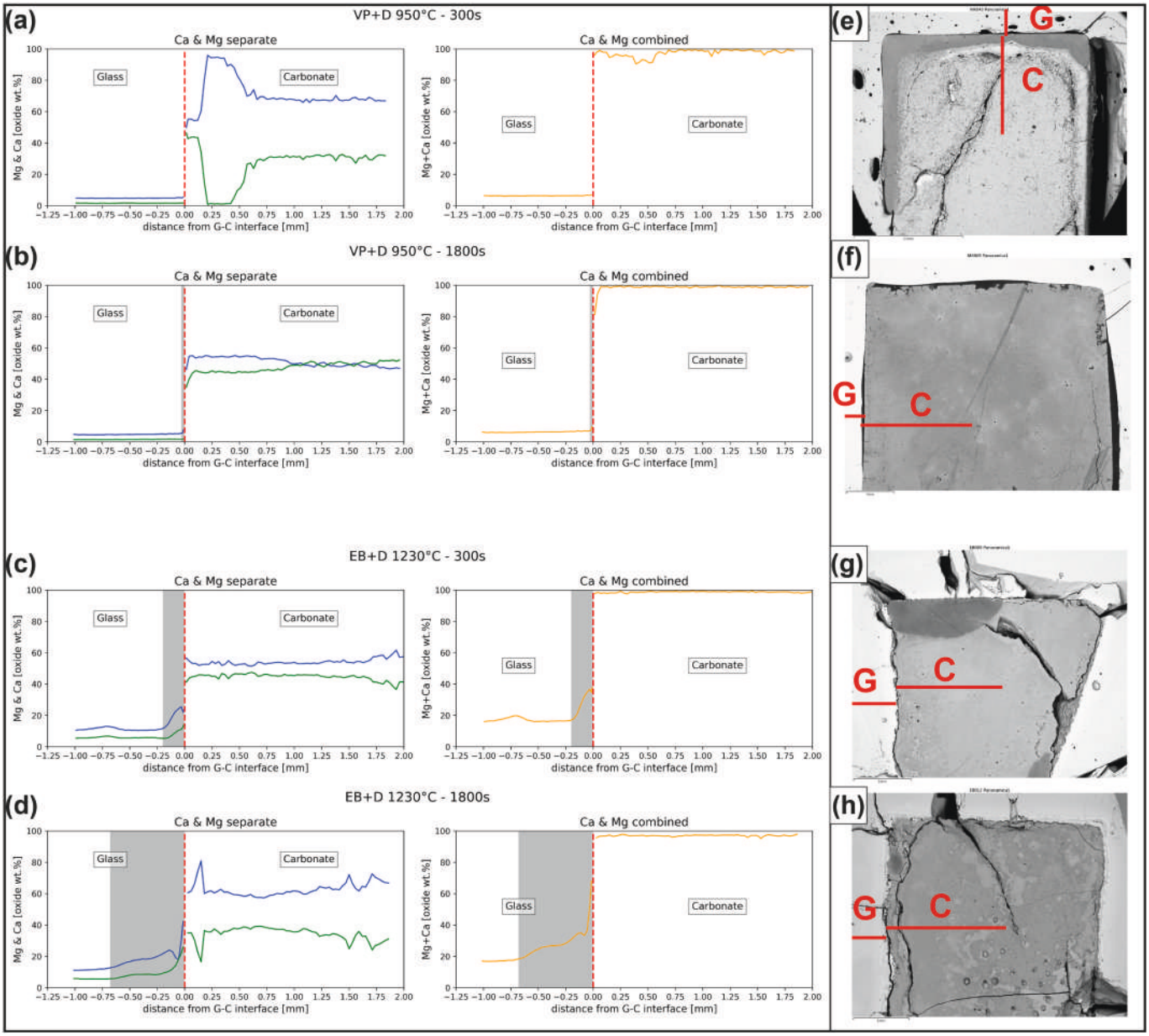

Fig. 9. Diffusion profiles of Ca & Mg in our experimental samples. Fig. 9 a&b show the diffusion profiles in the 300 s- and 1800s-experiments of the VP04 series (950 °C, phonolitic melt, dolomitic limestone, "large" sized clast), with the corresponding SEM-images to the right (Fig. 9 e&f). Fig. 9 c&d show the diffusion profiles in the 300 s- and 1800s-experiments of the EB02 series (1230 °C, basaltic melt, dolomitic limestone, "large" sized clast), with the corresponding SEM-images to the right (Fig. 9 g&h). The y-axis gives the Ca- and Mg-concentrations in weight % of the oxides, on the x-axis the distance from the glass-carbonate interface (red-dotted line) is given in mm. The green lines correspond to Mg-concentration, the blue lines to Ca-concentration and yellow line to combined Ca + Mg-concentrations. The diffusion-affected areas are highlighted as the grey areas. Note that the variable Ca- and Mg-concentrations are due to the heterogeneous nature of the dolomitic clast (as shown in Fig. 1). In the SEM-images (Fig. 9 e-h) the carbonate (C), the glass (G) and the lines corresponding to the diffusion measurement (red lines) are given. The length of this line within the carbonate is in between 1.8 and 2.1 mm in length, the line in the glass around 1 mm. (For interpretation of the references to colour in this figure legend, the reader is referred to the web version of this article.)

composition is the result of different onset temperatures of the decomposition reactions of Mg-carbonates, CaMg-carbonates and Ca-carbonates (~315 °C vs. ~538 °C vs. ~845 °C, respectively; Olszak-Humienik and Jablonski, 2015). This would also be in agreement with the thermal decomposition study on limestones by Marinoni et al. (2012), in which it was found that with increasing dolomitic content, the activation energy for the decomposition reaction is decreasing, leading to an earlier onset (i.e., at lower temperatures) of the decomposition reaction. Lastly, the melt composition and hence melt viscosity at 1230 °C (values given in Table 1) did not affect the decarbonation timescale (τ) in our experiments since the decarbonation is concluded in all 3 melts within the same time (i.e., ~150 s for dolomitic limestones, ~240 s for Ca-rich limestones; Fig. 5). In the previous short-term interaction studies at magma chamber level conditions (Deegan et al., 2010; Jolis et al., 2013; Blythe et al., 2015) and also in longer lasting experimental studies (e.g., Iacono-Marziano et al., 2008; Carter and Dasgupta, 2016) an effect of melt viscosity on the carbonate assimilation process was observed. In these studies, the carbonate assimilation was observed to be one process in which decarbonation and clast dissolution take place simultaneously. Our results indicate that the decarbonation process of ingested limestone clasts is a purely thermal process, during which CO_2 will be released due to heating of the limestone clasts above

Table 4
Summary of the main results of previous short-term magma carbonate interaction experiments at magma chamber conditions.

Main Results of previous short-term magma carbonate interaction studies (Deegan et al., 2010; Jolis et al., 2013; Blythe et al., 2015)	
Conditions	1200 °C, 0.5 GPa, sealed Pt capsules in piston cylinder apparatus, carbonate clast size: cubes with ≤3 mm side length, 0–300 s duration
Decarbonation Timescale	Due to exp. set-up not measurable separately
Clast Dissolution Timescale	in dry basaltic andesite: 270–300 s in hydrous basaltic andesite (2 wt% H_2O): 90 s in hydrous shoshonite (2 wt% H_2O): 0 s, i.e. during experimental heat-up
Main Controlling Parameter	Melt viscosity, H_2O-content and interaction time
Effect of H_2O	Faster clast dissolution due to reduced viscosity
Effect of P (0.5–1.0 GPa)	No measurable difference in clast dissolution timescale

their crystallographic stability. The magma acts only as heat source and its compositions, and hence its viscosity, has no further influence on the decarbonation rate.

The second process within carbonate assimilation, the chemical dissolution of the ingested clast via diffusion, has been measured along traverses from clast core into the glass by SEM analytical technique. In our experiments at 1230 °C Ca and Mg diffusion into the glass was first observed in the 300 s-experiments (Fig. 8), mostly due to the ingestion of the clast, during which we deformed the melt, creating voids around the clast, which inhibited direct contact of melt and ingested clast for a large part of the clasts surface. Once the melt relaxes (depending on melt viscosity), direct contact between clast and melt can be achieved and diffusion starts. In experiments at 950 °C in phonolitic melt, a relaxation of the melt around the clast was not achieved within the longest experimental duration, thus elemental diffusion was very restricted or absent. At higher temperature (i.e., at 1230 °C) both basaltic and phonolitic melts clearly show Ca and Mg diffusion into the melts for experimental durations ≥300 s. As expected, the width of the diffusion-affected area around the ingested clast increases with experimental runtime, but, considering melt composition, it is larger in the basaltic melt (W_D + 25% in 300 s-experiment and + 75% in 1800s-experiment). The general trend of more effective diffusion of Ca and Mg in lower viscosity melts in our experiments at atmospheric pressure is in agreement with numerous diffusion studies (e.g., Zhang et al., 2010 and references therein) and with the short-term magma-carbonate interaction study with applied pressure of Blythe et al. (2015). Contrarily to previous short-term interaction studies, in which the carbonate clast was completely dissolved within 270 s (Deegan et al., 2010; Jolis et al., 2013; Blythe et al., 2015), it remains macroscopically intact in our experiments even in the 1800s-experiments (Figs. 8 & 9).

Due to the limitations of our experimental approach (see Chapter 2.2.1) the interpretation of our dissolution results is not straightforward and a comparison to the previous experimental studies not possible. The absence of other dissolved volatile phases (like H_2O) in the magma, which enhance elemental diffusion (Zhang et al., 2010; González-García et al., 2017), slowed down the diffusion and therefore the dissolution process in our experiments. Deegan et al. (2010) conducted a series of experiments with hydrous and anhydrous glasses each and found the clast dissolution to be completed much earlier in hydrous melt experiments (90 s vs. 300 s). Still also in the anhydrous melt the limestone clast was completely dissolved within 300 s. Hence further processes and parameters need to be considered for the absence of complete limestone dissolution in our experiments (even after 1800 s, Figs. 8 & 9).

One major point regards the state of the magma (solid or liquid) in our experiments since we inserted the crucibles cold into the oven. In Fig. 3 we tried to measure and calculate theoretically the time needed to re-heat the crucibles. While the theoretical calculation makes some strong assumptions (constant c_p and h, uniform heating) its results (71 s to 950 °C and 54 s to 1230 °C, both times after start of experimental runtimes) need to be seen as very optimistic. More reasonable results were obtained with the thermocouple measurements (340 s to 950 °C and 175 s to 1230 °C, both times after start of experimental runtimes), but also these cannot account for the time needed to melt the glasses. At least, we can be confident that after 300 s for all experiments at 1230 °C a liquid state of the magma was achieved since the void between the limestone clast and the melt was closed and a direct contact between them established (Figs. 8 & 9). At this point the decarbonation process was already concluded (for both Ca-rich and dolomitic limestone and also for all magma compositions, Fig. 5) and CO_2 has very likely not permeated the melt in our experiments. This is a major difference to the closed system piston cylinder experiments of previous studies where the outwards movement of the bubbles was a main driver for enhanced mixing and mingling and hence for clast dissolution (Blythe et al., 2015).

Another major difference is the absence of pressure in our experiments, which might affect the dissolution timescale. In general, pressure is described as diffusion inhibiting (e.g., Watson, 1981; Zhang et al., 2010) which we would lead us to assume faster diffusion (and hence fast clast dissolution in lower pressure settings). There was, however, no perceivable change in the experimental results in a previous study in which experiments have been conducted at 0.5 and 1 GPa (Deegan et al., 2010). Also at 0.15 GPa the dissolution of the large carbonate component in magma-shale interaction experiments was completed rapidly (< 600 s, Deegan et al., 2022). From this few datapoints no clear dependency on pressure can be stipulated and further experiments at systematically varied pressures (0.1 MPa < P < 0.5 GPa) are needed to infer low-P rates of limestone dissolution.

Despite these limitations some important conclusions for limestone dissolution can be drawn from our experiments. To date, carbonate assimilation was observed to be only one process in which decarbonation and clast dissolution take place simultaneously. Our results show that at least for magma limestone interactions with the above-mentioned limitations the decarbonation and the clast dissolution act on two different timescales. In the absence of volatile phases, either dissolved or as free gas phase, the clast dissolution rates decline significantly compared to previous experiments leading to an incomplete dissolution even after 1800 s (i.e., Figs. 8 & 9 with t > 300 s). This highlights the previously found importance of magma composition and especially H_2O-content for the dissolution process (Deegan et al., 2010; Blythe et al., 2015). The absence of diffusion in the low temperature and the short-duration (t < 300 s) experiments highlights the importance of having a contact interface between the melt and the limestone clast.

4.1. Carbonate assimilation in the volcanic feeding system

Taking into account all the above considerations, we can make some qualitative assumptions on carbonate assimilation throughout the whole volcanic feeding system. The timescale of decarbonation of an ingested carbonate-bearing wall-rock, as expected, will mainly depend on temperature (at constant wall-rock composition) and not on the depth (hence, pressure) of the ingestion, as shown by the very similar timescales of decarbonation in this study (at atmospheric pressure) and in previous studies at 0.5 GPa (Deegan et al., 2010; Jolis et al., 2013; Blythe et al., 2015). The decarbonation process is also independent of melt composition, as shown in our experiments with phonolitic, shoshonitic, and basaltic melt composition (Fig. 5). La Spina et al. (2015) showed by numerical modelling, that the temperature during basaltic magma ascent initially decreases due to adiabatic cooling caused by gas expansion, but in even shallower settings might be increasing due to the release of latent heat from crystallization. Both processes together result in no major effect on the temperature (i.e., ±20 K variation) throughout the volcanic feeding system. This model does not consider wall-rock assimilation, which would consume energy, reduce the melt temperature significantly, inducing crystallization and increasing viscosity (e.g.,

Glazner, 2007). However, large amounts of limestone xenoliths (up to ~30 wt% in very proximal deposits, up to ~16 wt% in distal deposits) are found for example in the pumice deposits of the Plinian phase of the Pomici di Avellino eruption (EU3) of Somma-Vesuvius (Sulpizio et al., 2010). These limestones are usually situated in large bubbles within the pumices, which most likely prevented their chemical dissolution and a strong cooling effect on the magma. On the other hand, decarbonation seems to have occurred, forming the bubble around the limestone xenoliths. Anyway, the timescale of decarbonation will remain in *syn*-eruptive timescale, as evidenced by the highest value of τ of ~1000 s (or 16.5 min) in our 950 °C-experiments (Fig. 4). This implies that the decarbonation of ingested carbonate-bearing wall-rocks will happen syn-eruptively and independently of melt composition and depth of ingestion, and hence needs to be considered as syn-eruptive volatile source throughout the whole volcanic feeding system.

The timescale of clast dissolution within the volcanic feeding system is mainly dependent on magma composition, H_2O-content of the melt, clast size and interaction time (Deegan et al., 2010; Jolis et al., 2013; Blythe et al., 2015; Carter and Dasgupta, 2016; this study). Our results indicate that also the presence of a contact surface between melt and limestone clast, which might be absent in near-surface settings in nature due to already fragmenting magma or in deeper settings due to the formation of a CO_2 bubble around the limestone xenolith, is of importance. A dependence on pressure could not be resolved with this experimental approach and needs to be included in future studies with systematically varied p-conditions, H_2O-contents, temperatures and melt compositions which are needed to resolve the timescale of clast dissolution within the volcanic feeding system.

In summary, at depth (magma chamber level with P ~ 0.5 GPa and T ~ 1200 °C) clast dissolution and decarbonation seem to have the same or a very similar timescale. Towards Earth's surface the decarbonation rate will decrease due to the decreasing temperature of the magmatic mixture during ascent, which is amplified when assimilating wall-rocks on the way. The evolution of the clast dissolution timescale is rather unclear even so the lone datapoints of Deegan et al. (2022) for intermediate depths (i.e., pressure of 0.15 GPa) indicate no large changes in dissolution rate at constant temperature, H_2O-content and melt composition. We speculate that during ascent (i.e., when magma temperature decreases, viscosity increases and interaction time decreases) the clast dissolution rate will decelerate. But more experiments are needed to confirm this speculation.

4.2. Some implications for eruption dynamics

Transit time of magma within the feeding dyke during effusive (excluding lava dome formation) and explosive eruptions may well be in the order of minutes to tens of minutes (Humphreys et al., 2008; Castro and Dingwell, 2009; Costa et al., 2009b; Denis et al., 2013; Lloyd et al., 2014; Moussallam et al., 2019). This timescale of eruptive processes perfectly fits with the timescale of decarbonation in our and previous experiments, and it obliges to discuss some general feedbacks that interaction of rising magma with carbonate rocks can produce throughout the volcanic feeding system. Here, we focus especially on the effects of *syn*-eruptive decarbonation of the ingested limestone wall-rocks. We note again that this process has its limits. The thermal energy needed to heat the limestones above their crystallographic stability and to induce their breakdown (i.e., the release of CO_2) is derived from the magmatic body and therefore will lead to a cooling of the magma. A decreasing magma temperature will decelerate, or during extensive carbonate assimilation might even terminate, carbonate assimilation rate and/or magma ascent. In the following we assume carbonate assimilation remains within these limits.

Since CO_2 solubility, independently of magma composition, is close to zero at shallow depth (Mysen et al., 1975; Lowenstern, 2001; Botcharnikov et al., 2005; Vetere et al., 2011, 2014; Russell et al., 2012) virtually all of the CO_2 will form bubbles. Injection of volatiles into the magmatic mixture increases its buoyancy and driving pressure P_0 (Gudmundsson, 2012):

$$P_0 = (\rho_r - \rho_m) \bullet g \bullet h + \sigma + R_f \quad (3)$$

where ρ_r is the country rock density, ρ_m is the magma density, g is the gravity acceleration, h is the height of magma column, σ is the local stress acting perpendicular to the dyke, and R_f is the viscous resistance. The change in driving pressure influences the magma rising velocity (u) and momentum:

$$\rho_m \bullet u \bullet (du/dz) = -\rho_m \bullet g - \rho_m \bullet u^2 \bullet R_f - (dP_0/dz) \quad (4)$$

From eq. (4), it is evident how the shear rate (du/dz) critically depends on the pressure rate (dP_0/dz), and how any increase in the latter at equal magma column and conduit geometry (i.e., invariant weight and friction) produces an increase in shear rate that may cause to overpass the fragmentation threshold of the magma, following Maxwell's equation (Papale, 1999):

$$du/dz > k \bullet (G_\infty/m) \quad (5)$$

where k is a constant, G_∞ is the shear modulus at infinite frequency, and m is the viscosity. Relating these considerations back to magma-carbonate interactions in the volcanic feeding system, they imply that with the release of CO_2 and thus the decrease of the density of the magma-volatile mixture, the driving pressure of an eruption will increase, leading to faster magma ascent. Depending on the amount of CO_2 released into the magma, short term magma-carbonate interaction at shallow depths thus can strongly change the eruption dynamics, favouring eruptive style transitions (i.e., effusive to explosive) or prolonging the life of sustained explosive phases. To precisely assess which amount of carbonate assimilation may induce changes in eruptive style is beyond the scope of this paper and calls for further investigation. La Spina et al. (2022) conducted numerical modelling on the role of volatiles during basaltic magma ascent with excess volatile phases (CO_2 and H_2O). If the "excess" CO_2 is already pre-eruptively present in the melt it increases viscosity (due to higher crystal content and overall lower dissolved volatile phases), which balances the higher buoyancy and leads to a weaker correlation of CO_2 content and magma ascent rate. If the CO_2 is added from an external source, the increase in pressure resulting from adding CO_2 produces sufficient driving force to increase the mass eruption rate by one order of magnitude. According to their model the eruptive style would then change from highly explosive behaviour to lava fountaining. La Spina et al. (2022) conclude that if the volatiles cannot decouple efficiently from the melt at shallow depths (<6 km), due to higher magma viscosity, the magma is more likely to fragment and produce highly explosive eruptions even at low H_2O-contents. In any case, it is worth noting how Sottili et al. (2017) argued that the anomalous explosive behaviour of mafic high-K magmas is due to the *syn*-eruptive assimilation of carbonate wall-rock, and how Freda et al. (2011) introduced the idea of carbonate assimilation being the cause for a transition from effusive to explosive eruptive style. Finally, Massaro et al. (2018) and Pappalardo et al. (2018) suggested that the Plinian phases of the Pomici di Avellino and Pomici di Base eruption (respectively) at Somma-Vesuvius were prolonged by carbonate assimilation in the final part of the magmatic phase, due to the surplus of volatile supply to the magma. All these pieces of evidence highlight how magma-carbonate interaction needs to be considered in order to better understand the physics of eruptions from volcanoes residing on shallow carbonate bedrock.

5. Conclusions

The novel experimental approach used in this study allowed for detailed investigation of the decarbonation during syn-eruptive carbonate assimilation in near-surface settings and especially how its timescale is dependent on experimental parameters. Additionally, it

allowed for some limited statements on the clast dissolution process and its respective controlling parameters. By combining the results of our study with existing literature data, we could, for the first time, make some qualitative statements about syn-eruptive carbonate assimilation within the feeding dyke of an eruption.

The timescale of decarbonation was found to be mainly dependent on temperature and limestone composition and independent of melt composition. The magma acts only as heat source and the decarbonation timescale remains syn-eruptive (max. 16.5 min) throughout the studied 1230–950 °C temperature interval. This is an important finding for natural systems in which the temperature of the magma decreases during ascent and with increasing quantities of assimilated wall-rock. The liberated CO_2 from limestone decarbonation after ingestion in a magma will form an additional free volatile phase since CO_2 solubility is close to zero at shallow depths (e.g., Lowenstern, 2001). Simplified considerations show how injected volatiles increase the buoyancy and ascent velocity of a magmatic mixture (Gudmundsson, 2012). The externally derived "excess" CO_2 may increase the driving pressure of an eruption, leading to larger mass eruption rate (La Spina et al., 2022), which might be realized by a prolonged eruption duration as suggested by Massaro et al. (2018) and Pappalardo et al. (2018) for the Plinian phases of the Pomici di Avellino and Pomici di Base eruptions of Somma-Vesuvius, respectively. Depending on the efficiency of the decoupling of the volatile phases from the melt at shallow depths (<6 km), hence depending on melt viscosity, the increased volatile budget may lead to highly explosive eruptions or lava fountaining (La Spina et al., 2022).

On the other hand, the clast dissolution process in our experiments is mainly dependent on melt composition, with more silica-undersaturated melt compositions allowing for more extensive clast dissolution. Though difficult to compare the two experimental procedures in terms of clast dissolution, it is evident that in absence of a dissolved volatile phase and hence at higher melt viscosities the dissolution process via diffusion is strongly decelerated (Deegan et al., 2010; Zhang et al., 2010; Blythe et al., 2015; this study). Besides the melt composition, its H_2O-content and interaction time, a seemingly trivial but nevertheless important requirement for clast dissolution is the establishment of a contact surface between melt and ingested limestone clast. In nature the formation of CO_2 bubbles, especially in higher viscosity melts, around the ingested limestone clast might prevent the formation of a large contact surface between melt and limestone clast. This process might explain the large quantities of limestone xenoliths (up to ~30 wt%) in the pumice deposits of the Pomici di Avellino Plinian phase (Sulpizio et al., 2010), since energy in form of heat of the magma was only consumed to decompose the limestone clast but not to chemically dissolve it.

These considerations highlight the need for magma-limestone interaction experiments with systematically varied pressure between atmospheric conditions and 0.5 GPa and the need to generally consider shallow syn-eruptive magma wall-rock interactions in magma ascent modelling, especially if the volcanic systems are underlain by bedrocks that are able to release volatile phases.

Funding

This research did not receive any specific grant from funding agencies in the public, commercial, or non-for-profit sectors.

Declaration of Competing Interest

The authors declare that they have no known competing financial interests or personal relationships that could have appeared to influence the work reported in this paper.

Data availability

The data used in this study is attached as Supplementary Table.

Acknowledgements

The authors thank Angela Bertinelli for providing the microporous Ca-rich limestone sample for this experimental study. MK thanks Nicola Mongelli for the technical assistance during the SEM-measurements. FV acknowledges UniSi-MUR F_Cur 2022 fundings.

Appendix A. Supplementary data

Supplementary data to this article can be found online at https://doi.org/10.1016/j.chemgeo.2023.121724.

References

Andersen, R., Bates, L., Johnson, E., Morris, J.F., 2015. Packed bed thermal energy storage: a simplified experimentally validated model. J. Energy Stor. 4, 14–23. https://doi.org/10.1016/j.est.2015.08.007.

Andriani, G.F., Walsh, N., 2007. Rocky coast geomorphology and erosional processes: a case study along the Murgia coastline South of Bari, Apulia - SE Italy. Geomorphology 87, 224–238. https://doi.org/10.1016/j.geomorph.2006.03.033.

Blank, J.G., Brooker, R.A., 1994. Experimental studies of carbon dioxide in silicate melts: solubility speciation and stable carbon isotope behaviour. Mineral. Soc. Am. Rev. Mineral. 30, 157–186.

Blythe, L.S., Deegan, F.M., Freda, C., Jolis, E.M., Masotta, M., Misiti, V., Taddeucci, J., Troll, V.R., 2015. CO2 bubble generation and migration during magma–carbonate interaction. Contrib. Mineral. Petrol. 169, 1–16. https://doi.org/10.1007/s00410-015-1137-4.

Botcharnikov, R., Freise, M., Holtz, F., Behrens, H., 2005. Solubility of C-O-H mixtures in natural melts: new experimantal data and application range of recent models. Ann. Geophys. 48, 633–646.

Buono, G., Pappalardo, L., Harris, C., Edwards, B.R., Petrosino, P., 2020. Magmatic stoping during the caldera-forming Pomici di Base eruption (Somma-Vesuvius, Italy) as a fuel of eruption explosivity. Lithos 370–371. https://doi.org/10.1016/j.lithos.2020.105628.

Caggiani, M.C., Ditaranto, N., Guascito, M.R., Acquafredda, P., Laviano, R., Giannossa, L. C., Mutino, S., Mangone, A., 2015. Combined analysis of enamelled and gilded glassware from Frederick II Castle at Melfi (Italy) to identify technology and raw materials. X-Ray Spectrom. 44, 191–200. https://doi.org/10.1002/xrs.2594.

Carr, B.B., Clarke, A.B., de' Michieli Vitturi, M., 2018. Earthquake induced variations in extrusion rate: a numerical modeling approach to the 2006 eruption of Merapi Volcano (Indonesia). Earth Planet. Sci. Lett. 482, 377–387. https://doi.org/10.1016/j.epsl.2017.11.019.

Carr, B.B., Clarke, A.B., de' Michieli Vitturi, M., 2020. Volcanic conduit controls on effusive-explosive transitions and the 2010 eruption of Merapi Volcano (Indonesia). J. Volcanol. Geotherm. Res. 392 https://doi.org/10.1016/j.jvolgeores.2019.106767.

Carter, L.B., Dasgupta, R., 2015. Hydrous basalt-limestone interaction at crustal conditions: Implications for generation of ultracalcic melts and outflux of CO2 at volcanic arcs. Earth Planet. Sci. Lett. 427, 202–214. https://doi.org/10.1016/j.epsl.2015.06.053.

Carter, L.B., Dasgupta, R., 2016. Effect of melt composition on crustal carbonate assimilation: Implications for the transition from calcite consumption to skarnification and associated CO2 degassing. Geochem. Geophys. Geosyst. 17, 3893–3916. https://doi.org/10.1002/2016GC006444.

Castro, J.M., Dingwell, D.B., 2009. Rapid ascent of rhyolitic magma at Chaitén volcano, Chile. Nature 461, 780–783. https://doi.org/10.1038/nature08458.

Chadwick, J.P., Troll, V.R., Ginibre, C., Morgan, D., Gertisser, R., Waight, T.E., Davidson, J.P., 2007. Carbonate assimilation at Merapi Volcano, Java, Indonesia: Insights from crystal isotope stratigraphy. J. Petrol. 48, 1793–1812. https://doi.org/10.1093/petrology/egm038.

Cosentino, D., Cipollari, P., Marsili, P., Scrocca, D., 2010. Geology of the central Apennines: a regional review. J. Virtual Explor. 36 https://doi.org/10.3809/jvirtex.2010.00223.

Costa, A., 2005. Viscosity of high crystal content melts: dependence on solid fraction. Geophys. Res. Lett. 32 https://doi.org/10.1029/2005GL024303.

Costa, A., Melnik, O., Sparks, R.S.J., 2007. Controls of conduit geometry and wallrock elasticity on lava dome eruptions. Earth Planet. Sci. Lett. 260, 137–151. https://doi.org/10.1016/j.epsl.2007.05.024.

Costa, A., Caricchi, L., Bagdassarov, N., 2009a. A model for the rheology of particle-bearing suspensions and partially molten rocks. Geochem. Geophys. Geosyst. 10 https://doi.org/10.1029/2008GC002138.

Costa, A., Sparks, R.S.J., Macedonio, G., Melnik, O., 2009b. Effects of wall-rock elasticity on magma flow in dykes during explosive eruptions. Earth Planet. Sci. Lett. 288, 455–462. https://doi.org/10.1016/j.epsl.2009.10.006.

Cross, J.K., Tomlinson, E.L., Giordano, G., Smith, V.C., de Benedetti, A.A., Roberge, J., Manning, C.J., Wulf, S., Menzies, M.A., 2014. High level triggers for explosive mafic volcanism: Albano Maar, Italy. Lithos 190–191, 137–153. https://doi.org/10.1016/j.lithos.2013.11.001.

Dallai, L., Cioni, R., Boschi, C., D'Oriano, C., 2011. Carbonate-derived CO2 purging magma at depth: Influence on the eruptive activity of Somma-Vesuvius, Italy. Earth Planet. Sci. Lett. 310, 84–95. https://doi.org/10.1016/j.epsl.2011.07.013.

Deegan, F.M., Troll, V.R., Freda, C., Misiti, V., Chadwick, J.P., McLeod, C.L., Davidson, J. P., 2010. Magma-carbonate interaction processes and associated CO2 release at

Merapi volcano, Indonesia: Insights from experimental petrology. J. Petrol. 51, 1027–1051. https://doi.org/10.1093/petrology/egq010.
Deegan, F.M., Bédard, J.H., Grasby, S.E., Dewing, K., Geiger, H., Misiti, V., Capriolo, M., Callegaro, S., Svensen, H.H., Yakymchuk, C., Aradi, L.E., Freda, C., Troll, V.R., 2022. Magma-shale interaction in large igneous Provinces: implications for climate warming and sulfide genesis. J. Petrol. 63, 1–10. https://doi.org/10.1093/petrology/egac094.
del Moro, A., Fulignati, P., Marianelli, P., Sbrana, A., 2001. Magma contamination by direct wall rock interaction: constraints from xenoliths from the walls of a carbonate-hosted magma chamber (Vesuvius 1944 eruption). J. Volcanol. Geotherm. Res. 112, 15–24.
Denis, C.M.M., Demouchy, S., Shaw, C.S.J., 2013. Evidence of dehydration in peridotites from Eifel Volcanic Field and estimates of the rate of magma ascent. J. Volcanol. Geotherm. Res. 258, 85–99. https://doi.org/10.1016/j.jvolgeores.2013.04.010.
di Rocco, T., Freda, C., Gaeta, M., Mollo, S., Dallai, L., 2012. Magma chambers emplaced in carbonate substrate: Petrogenesis of skarn and cumulate rocks and implications for CO 2 degassing in volcanic areas. J. Petrol. 53, 2307–2332. https://doi.org/10.1093/petrology/egs051.
Escardino, A., Garcia-Ten, J., Feliu, C., 2008. Kinetic study of calcite particle (powder) thermal decomposition: part I. J. Eur. Ceram. Soc. 28, 3011–3020. https://doi.org/10.1016/j.jeurceramsoc.2008.05.017.
Freda, C., Gaeta, M., Misiti, V., Mollo, S., Dolfi, D., Scarlato, P., 2008. Magma-carbonate interaction: an experimental study on ultrapotassic rocks from Alban Hills (Central Italy). Lithos 101, 397–415. https://doi.org/10.1016/j.lithos.2007.08.008.
Freda, C., Gaeta, M., Giaccio, B., Marra, F., Palladino, D.M., Scarlato, P., Sottili, G., 2011. CO2-driven large mafic explosive eruptions: the Pozzolane Rosse case study from the Colli Albani Volcanic District (Italy). Bull. Volcanol. 73, 241–256. https://doi.org/10.1007/s00445-010-0406-3.
Giordano, D., Russell, J.K., Dingwell, D.B., 2008. Viscosity of magmatic liquids: a model. Earth Planet. Sci. Lett. 271, 123–134. https://doi.org/10.1016/j.epsl.2008.03.038.
Glazner, A.F., 2007. Thermal limitations on incorporation of wall rock into magma. Geology 35, 319–322. https://doi.org/10.1130/G23134A.1.
Goff, F., Love, S.P., Warren, R.G., Counce, D., Obenholzner, J., Siebe, C., Schmidt, S.C., 2001. Passive infrared remote sensing evidence for large, intermittent CO emissions at Popocatepetl volcano, Mexicó. Chem. Geol. 177, 133–156.
González-García, D., Behrens, H., Petrelli, M., Vetere, F., Morgavi, D., Zhang, C., Perugini, D., 2017. Water-enhanced interdiffusion of major elements between natural shoshonite and high-K rhyolite melts. Chem. Geol. 466, 86–101. https://doi.org/10.1016/j.chemgeo.2017.05.023.
Gozzi, F., Gaeta, M., Freda, C., Mollo, S., di Rocco, T., Marra, F., Dallai, L., Pack, A., 2014. Primary magmatic calcite reveals origin from crustal carbonate. Lithos 190–191, 191–203. https://doi.org/10.1016/j.lithos.2013.12.008.
Gudmundsson, A., 2012. Magma chambers: Formation, local stresses, excess pressures, and compartments. J. Volcanol. Geotherm. Res. 237–238, 19–41. https://doi.org/10.1016/j.jvolgeores.2012.05.015.
Holloway, John R., Blank, J.G., 1994. Application of experimental results to C-O-H species in natural melts. In: Carroll, M.R., Holloway, J.R. (Eds.), Volatiles in Magma. Mineralogical Society of America, pp. 187–230.
Humphreys, M.C.S., Menand, T., Blundy, J.D., Klimm, K., 2008. Magma ascent rates in explosive eruptions: Constraints from H2O diffusion in melt inclusions. Earth Planet. Sci. Lett. 270, 25–40. https://doi.org/10.1016/j.epsl.2008.02.041.
Iacono-Marziano, G., Gaillard, F., Pichavant, M., 2007. Limestone assimilation and the origin of CO2 emissions at the Alban Hills (Central Italy): Constraints from experimental petrology. J. Volcanol. Geotherm. Res. 166, 91–105. https://doi.org/10.1016/j.jvolgeores.2007.07.001.
Iacono-Marziano, G., Gaillard, F., Pichavant, M., 2008. Limestone assimilation by basaltic magmas: an experimental re-assessment and application to Italian volcanoes. Contrib. Mineral. Petrol. 155, 719–738. https://doi.org/10.1007/s00410-007-0267-8.
Iacono-Marziano, G., Gaillard, F., Scaillet, B., Pichavant, M., Chiodini, G., 2009. Role of non-mantle CO2 in the dynamics of volcano degassing: the Mount Vesuvius example. Geology 37, 319–322. https://doi.org/10.1130/G25446A.1.
Janik, C.J., Goff, F., Fahlquist, L., Adams, A.I., Alfredo Roldan, M., Chipera, S.J., Trujillo, P.E., Counce, D., 1992. Hydrogeochemical exploration of geothermal prospects in the Tecuamburro Volcano region, Guatemala. Geothermics 21, 447–481. https://doi.org/10.1016/0375-6505(92)90002-Q.
Jolis, E.M., Freda, C., Troll, V.R., Deegan, F.M., Blythe, L.S., McLeod, C.L., Davidson, J.P., 2013. Experimental simulation of magma-carbonate interaction beneath Mt. Vesuvius, Italy. Contrib. Mineral. Petrol. 166, 1335–1353. https://doi.org/10.1007/s00410-013-0931-0.
Knuever, M., Sulpizio, R., Mele, D., Costa, A., 2022. Magma–rock interactions: a review of their influence on magma rising processes with emphasis on short-timescale assimilation of carbonate rocks. Geol. Soc. Lond., Spec. Publ. SP520-2021–177 https://doi.org/10.1144/sp520-2021-177.
La Spina, G., Burton, M., de' Michieli Vitturi, M., 2015. Temperature evolution during magma ascent in basaltic effusive eruptions: A numerical application to Stromboli volcano. Earth Planet. Sci. Lett. 426, 89–100. https://doi.org/10.1016/j.epsl.2015.06.015.
La Spina, G., Arzilli, F., Burton, M.R., Polacci, M., Clarke, A.B., 2022. Role of volatiles in highly explosive basaltic eruptions. Commun. Earth Environ. 3, 156–168. https://doi.org/10.1038/s43247-022-00479-6.
Lloyd, A.S., Ruprecht, P., Hauri, E.H., Rose, W., Gonnermann, H.M., Plank, T., 2014. NanoSIMS results from olivine-hosted melt embayments: Magma ascent rate during explosive basaltic eruptions. J. Volcanol. Geotherm. Res. 283, 1–18. https://doi.org/10.1016/j.jvolgeores.2014.06.002.
Lowenstern, J.B., 2001. Carbon dioxide in magmas and implications for hydrothermal systems. Mineral. Deposita 36, 490–502. https://doi.org/10.1007/s001260100185.
Marinoni, N., Allevi, S., Marchi, M., Dapiaggi, M., 2012. A kinetic study of thermal decomposition of limestone using in situ high temperature X-ray powder diffraction. J. Am. Ceram. Soc. 95, 2491–2498. https://doi.org/10.1111/j.1551-2916.2012.05207.x.
Massaro, S., Costa, A., Sulpizio, R., 2018. Evolution of the magma feeding system during a Plinian eruption: the case of Pomici di Avellino eruption of Somma–Vesuvius, Italy. Earth Planet. Sci. Lett. 482, 545–555. https://doi.org/10.1016/j.epsl.2017.11.030.
Massaro, S., Costa, A., Sulpizio, R., Coppola, D., Capra, L., 2019. Cyclic activity of the Fuego de Colima volcano (Mexico): Insights from satellite thermal data and nonlinear models. Solid Earth 10, 1429–1450. https://doi.org/10.5194/se-10-1429-2019.
Mollo, S., Gaeta, M., Freda, C., di Rocco, T., Misiti, V., Scarlato, P., 2010. Carbonate assimilation in magmas: a reappraisal based on experimental petrology. Lithos 114, 503–514. https://doi.org/10.1016/j.lithos.2009.10.013.
Morris, R., Canil, D., 2022. CO2 transport at shallow depths in arc magmas: evidence from unique orbicular dikes in the Jurassic Bonanza arc, Vancouver Island, Canada. Contrib. Mineral. Petrol. 177 https://doi.org/10.1007/s00410-021-01852-y.
Moussallam, Y., Rose-Koga, E.F., Koga, K.T., Médard, E., Bani, P., Devidal, J.L., Tari, D., 2019. Fast ascent rate during the 2017–2018 Plinian eruption of Ambae (Aoba) volcano: a petrological investigation. Contrib. Mineral. Petrol. 174 https://doi.org/10.1007/s00410-019-1625-z.
Musu, A., Caricchi, L., Perugini, D., Corsaro, R.A., Vetere, F., Petrelli, M., 2021. Crystal zoning patterns: competition between crystal growth and elements diffusion. In: EGU General Assembly 2021, online, 19–30 Apr 2021, EGU21-10053. https://doi.org/10.5194/egusphere-egu21-10053.
Mysen, B.O., Arculus, R.J., Eggler, D.H., 1975. Solubility of carbon dioxide in melts of andesite, tholeiite, and olivine nephelinite composition to 30 kbar pressure. Contrib. Mineral. Petrol. 53, 227–239.
Olszak-Humienik, M., Jablonski, M., 2015. Thermal behavior of natural dolomite. J. Therm. Anal. Calorim. 119, 2239–2248. https://doi.org/10.1007/s10973-014-4301-6.
Papale, P., 1999. Modeling of the solubility of a two-component H 2 O CO 2 fluid in silicate liquids. Am. Mineral. 84, 477–492.
Papale, P., Moretti, R., Barbato, D., 2006. The compositional dependence of the saturation surface of H2O + CO2 fluids in silicate melts. Chem. Geol. 229, 78–95. https://doi.org/10.1016/j.chemgeo.2006.01.013.
Pappalardo, L., Buono, G., Fanara, S., Petrosino, P., 2018. Combining textural and geochemical investigations to explore the dynamics of magma ascent during Plinian eruptions: a Somma–Vesuvius volcano (Italy) case study. Contrib. Mineral. Petrol. 173 https://doi.org/10.1007/s00410-018-1486-x.
Pisello, A., De Angelis, S., Ferrari, M., Porreca, M., Vetere, F.P., Behrens, H., De Sanctis, M.C., Perugini, D., 2022a. Visible and near-InfraRed (VNIR) reflectance of silicate glasses: Characterization of a featureless spectrum and implications for planetary geology. Icarus 374, 114801. https://doi.org/10.1016/j.icarus.2021.114801.
Pisello, A., Ferrari, M., De Angelis, S., Vetere, F.P., Porreca, M., Stefani, S., Perugini, D., 2022b. Reflectance of silicate glasses in the mid-infrared region (MIR): Implications for planetary research. Icarus 388, 115222. https://doi.org/10.1016/j.icarus.2022.115222.
Russell, J.K., Porritt, L.A., Lavallé, Y., Dingwell, D.B., 2012. Kimberlite ascent by assimilation-fuelled buoyancy. Nature 481, 352–356. https://doi.org/10.1038/nature10740.
Scandone, R., Bellucci, F., Lirer, L., Rolandi, G., 1991. The structure of the Campanian Plain and the activity of the Neapolitan volcanoes (Italy). J. Volcanol. Geotherm. Res. 48, 1–31.
Sottili, G., Taddeucci, J., Palladino, D.M., 2010. Constraints on magma-wall rock thermal interaction during explosive eruptions from textural analysis of cored bombs. J. Volcanol. Geotherm. Res. 192, 27–34. https://doi.org/10.1016/j.jvolgeores.2010.02.003.
Sottili, G., Fanara, S., Silleni, A., Palladino, D.M., Schmidt, B.C., 2017. CO2-crystal wettability in potassic magmas: implications for eruptive dynamics in light of experimental evidence for heterogeneous nucleation. Geophys. J. Int. 209, 688–694. https://doi.org/10.1093/gji/ggx039.
Sulpizio, R., Cioni, R., di Vito, M.A., Mele, D., Bonasia, R., Dellino, P., 2010. The Pomici di Avellino eruption of Somma-Vesuvius (3.9 ka bp). Part I: Stratigraphy, compositional variability and eruptive dynamics. Bull. Volcanol. 72, 539–558. https://doi.org/10.1007/s00445-009-0339-x.
Thibault, Y., Holloway, J.R., 1994. Solubility of CO2 in a Ca-rich leucitite: effects of pressure, temperature, and oxygen fugacity. Contrib. Mineral. Petrol. 116, 216–224.
Troll, V.R., Hilton, D.R., Jolis, E.M., Chadwick, J.P., Blythe, L.S., Deegan, F.M., Schwarzkopf, L.M., Zimmer, M., 2012a. Crustal CO2 liberation during the 2006 eruption and earthquake events at Merapi volcano, Indonesia. Geophys. Res. Lett. 39 https://doi.org/10.1029/2012GL051307.
Troll, V.R., Klügel, A., Longpre, M.A., Burchardt, S., Deegan, F.M., Carracedo, J.C., Wiesmaier, S., Kueppers, U., Dahren, B., Blythe, L.S., Hansteen, T.H., Freda, C., Budd, D.A., Jolis, E.M., Jonsson, E., Meade, F.C., Harris, C., Berg, S.E., Mancini, L., Polacci, M., Pedroza, K., 2012b. Floating stones off El Hierro, Canary Islands: Xenoliths of pre-island sedimentary origin in the early products of the October 2011 eruption. Solid Earth 3, 97–110. https://doi.org/10.5194/se-3-97-2012.
Vetere, F., Behrens, H., Misiti, V., Ventura, G., Holtz, F., de Rosa, R., Deubener, J., 2007. The viscosity of shoshonitic melts (Vulcanello Peninsula, Aeolian Islands, Italy): Insight on the magma ascent in dikes. Chem. Geol. 245, 89–102. https://doi.org/10.1016/j.chemgeo.2007.08.002.

Vetere, F., Botcharnikov, R.E., Holtz, F., Behrens, H., de Rosa, R., 2011. Solubility of H2O and CO2 in shoshonitic melts at 1250°C and pressures from 50 to 400MPa: Implications for Campi Flegrei magmatic systems. J. Volcanol. Geotherm. Res. 202, 251–261. https://doi.org/10.1016/j.jvolgeores.2011.03.002.

Vetere, F., Sato, H., Ishibashi, H., de Rosa, R., Donato, P., 2013. Viscosity changes during crystallization of a shoshonitic magma: New insights on lava flow emplacement. J. Mineral. Petrol. Sci. 108, 144–160. https://doi.org/10.2465/jmps.120724.

Vetere, F., Holtz, F., Behrens, H., Botcharnikov, R.E., Fanara, S., 2014. The effect of alkalis and polymerization on the solubility of H2O and CO2 in alkali-rich silicate melts. Contrib. Mineral. Petrol. 167, 1014. https://doi.org/10.1007/s00410-014-1014-6.

Vetere, F., Iezzi, G., Behrens, H., Holtz, F., Ventura, G., Misiti, V., Cavallo, A., Mollo, S., Dietrich, M., 2015a. Glass forming ability and crystallisation behaviour of sub-alkaline silicate melts. Earth Sci. Rev. 150, 25–44. https://doi.org/10.1016/j.earscirev.2015.07.001.

Vetere, F., Petrelli, M., Morgavi, D., Perugini, D., 2015b. Dynamics and time evolution of a shallow plumbing system: the 1739 and 1888-90 eruptions, Vulcano Island, Italy. J. Volcanol. Geotherm. Res. 306, 74–82. https://doi.org/10.1016/j.jvolgeores.2015.09.024.

Watson, E.B., 1981. Diffusion in magmas at depth in the Earth: the effects of pressure and dissolved H2O. Earth Planet. Sci. Lett. 52, 291–301.

Whitley, S., Gertisser, R., Halama, R., Preece, K., Troll, V.R., Deegan, F.M., 2019. Crustal CO2 contribution to subduction zone degassing recorded through calc-silicate xenoliths in arc lavas. Sci. Rep. 9 https://doi.org/10.1038/s41598-019-44929-2.

Zhang, Y., Ni, H., Chen, Y., 2010. Diffusion data in silicate melts. Rev. Mineral. Geochem. 72, 311–408. https://doi.org/10.2138/rmg.2010.72.8.